research report

Monotonic and Cyclic Tests of Long Steel-Frame Shear Walls with Openings

RESEARCH REPORT RP99-2

1999
REVISION 2007

American Iron and Steel Institute

Steel Framing Alliance™
Steel. The Better Builder.

DISCLAIMER

The material contained herein has been developed by researchers based on their research findings and is for general information only. The information in it should not be used without first securing competent advice with respect to its suitability for any given application. The publication of the information is not intended as a representation or warranty on the part of the American Iron and Steel Institute, Steel Framing Alliance, or of any other person named herein, that the information is suitable for any general or particular use or of freedom from infringement of any patent or patents. Anyone making use of the information assumes all liability arising from such use.

PREFACE

This report presents the results of monotonic and cyclic tests of sixteen full-size, cold-formed steel-framed shear walls sheathed with oriented strand board, with and without openings.

The findings provided a basis for continued research and development efforts, leading to the establishment of provisions for cold-formed steel-framed Type II shear walls.

Research Team
Steel Framing Alliance

Monotonic and Cyclic Tests of Long Steel-Frame Shear Walls with Openings

Virginia Polytechnic Institute and State University
Department of Wood Science and Forests Products
Brooks Forest Products Research Center
Timber Engineering Center
1650 Ramble Road
Blacksburg, Virginia 24061-0503

Report No. TE-1999-001

by:

A.J. Salenikovich
Research Assistant

J.D. Dolan
Associate Professor of Wood Engineering

And

W. S. Easterling
Associate Professor of Civil Engineering

Submitted to:
The American Iron & Steel Institute
Washington, DC

March, 1999

ABSTRACT

Presented are results of monotonic and cyclic tests of sixteen full-size, cold-formed steel-frame shear walls sheathed with oriented strandboard, with and without openings. Walls of five configurations with sheathing area ratio ranging from 0.3 to 1.0 were tested. The specimens were 12-m (40-ft.) long and 2.4-m (8-ft.) high with 11-mm (7/16-in.) OSB sheathing. Two walls had additional 13-mm (0.5-in.) gypsum wallboard sheathing. All specimens were tested in horizontal position with no dead load applied in the plane of the wall. Resistance of walls was compared with predictions of the perforated shear wall design method (already developed for wood-framed walls) in order to validate that the perforated shear wall method is valid regardless of framing material.

Results of the study revealed that steel-framed walls had a similar load capacity to wood-frame walls. In steel framing, bending of framing elements and head pull-through of sheathing screws was the predominant failure mode, compared to withdrawal, head pull through, and fatigue for wood-framed walls. Gypsum sheathing added 30% to stiffness and strength of fully sheathed walls in monotonic tests, however contribution of gypsum wallboard in other loading circumstances remains questionable. Predictions of the perforated shear wall method were conservative.

TABLE OF CONTENTS

LIST OF TABLES

LIST OF FIGURES

INTRODUCTION

Light-frame shear walls are a primary element in the lateral force-resisting system in residential construction. Both prescriptive and engineering methods have yet been developed for cold-formed steel construction. Shear wall design values for segmented walls of cold-formed steel construction have been included in the three model building codes for the United States. The perforated shear wall method has also been adopted by the National Building Code and draft of the International Building Code. If similar sheathing materials and connections are used for wood- and steel- frame shear walls, it is reasonable to assume similar performance for both types of frames. This study validates that the perforated shear wall method for design of shear walls is also valid for cold-formed steel shear walls.

Traditional wood panel sheathed shear wall design for wood and steel framing requires fully-sheathed wall sections to be restrained against overturning. Their behavior is often considered analogous to a deep cantilever beam with the end framing members acting as "flanges" or "chords" to resist overturning moment forces and the panels acting as a "web" to resist shear. This analogy is generally considered appropriate for wind and seismic design. Overturning, shear restraint, and chord forces are calculated using principles of engineering mechanics. While shear resistance can be calculated using engineering mechanics as well, tabulated shear resistance values for varying fastener schedules have been introduced in the codes and are typically used.

Traditional design of exterior shear walls containing openings, for windows and doors, involves the use of multiple shear wall segments. Each full-height shear wall segment is required to have overturning restraint supplied by structure weight and/or mechanical anchors. The shear capacity of a wall must equal the sum of the individual full-height segment shear capacities. Sheathing above and below openings is not considered to contribute to the overall performance of the wall.

An alternate empirical-based approach to the design of wood-framed shear walls with openings is the perforated shear wall method which appears in Chapter 23 of the *Standard Building Code 1996 Revised Edition* (SBC) [17], the *International Building Code* final draft [8], and the *Wood Frame Construction Manual for One- and Two- Family Dwellings - 1995 High Wind Edition* (WFCM) [1]. The perforated shear wall method consists of a combination of prescriptive provisions and empirical adjustments to design values in shear wall selection tables for the design of shear wall segments containing openings. Shear walls designed using this method, must be anchored only at the wall ends, not each wall segment.

Japanese researchers [20,21] performed a number of monotonic tests on one-third scale models of wood-frame shear walls and proposed a basis for the perforated shear wall method. A number of monotonic and reverse-cyclic tests on 12.2-m (40-ft.) long wood-frame walls performed by Johnson [10] and Heine [7] demonstrated conservative nature of the proposed method. This study provides information about the performance of long, full-sized, perforated shear walls with cold-formed steel framing tested under monotonic and reverse-cyclic loads. Monotonic tests serve as a basis for establishing design values in wind design. Cyclic tests are performed to establish conservative estimates of performance during a seismic event.

Objectives

Results of monotonic and cyclic tests of full-size cold-formed steel-frame shear walls meeting the requirements of the perforated shear wall method are reported. The objectives of this study were to determine the effects of (a) size of openings, (b) cyclic loading, (c) gypsum drywall sheathing and steel framing on shear wall performance and to compare the strength of walls with predictions of the perforated shear wall method.

BACKGROUND

Design values for cold-formed steel-framed shear walls are based on monotonic and cyclic tests of shear walls. The tests were traditionally conducted on 2.4 x 2.4 m (8 x 8 ft.) and 1.2 x 2.4 m (4 x 8 ft.) wall specimens, similar to those used for wood-framed shear walls. Seismic and wind design values are based on testing conducted by Serrette, et al. [16, 17], which included monotonic and cyclic tests of walls sheathed with plywood, oriented strandboard, and gypsum wallboard on both 1.2 × 2.4 m (4 × 8 ft.) and 2.4 × 2.4 m (8 × 8 ft.) wall specimens.

The perforated shear wall design method for wood-frame shear walls appearing in the SBC, IBC, and WFCM is based on an empirical equation, which relates the strength of a shear wall segment with openings to one without openings. Adjustment factors in Table 2313.2.2 in the SBC and Supplement Table 3B in the WFCM are used to reduce the strength or increase the required length of a traditional fully sheathed shear wall segment to account for the presence of openings.

In accordance with SBC and WFCM, and for the purposes of this study, a perforated shear wall must include the following components:

1) Structural sheathing, including areas above and below window and door openings;
2) Mechanical shear restraint capable of resisting the shear capacity of each segment;
3) Tie-downs at the ends of the wall to provide overturning restraint and maintain a continuous load path to the foundation where any plan discontinuities occur in the wall line;
4) Minimum length of full-height sheathing at each end of the wall (Based on height-to-length ratios for blocked shear wall segments as prescribed by the applicable building code).

Prescriptive provisions and empirical adjustments are based on results of various studies conducted on shear walls with openings. Many of the prescriptive provisions are necessary to meet conditions for which walls in previous studies were tested. Empirically derived adjustment factors, or shear capacity ratios, for the perforated shear wall method take roots in works of

Japanese researchers [18, 19, 20]. To determine the shear capacity ratio, Sugiyama and Matsumoto [19] defined the sheathing area ratio:

$$r = \frac{1}{1 + \frac{A_0}{H \sum L_i}} \tag{1}$$

where: $A_0 = \sum A_i$, total area of openings, H = height of wall, and $\sum L_i$ = sum of the length of full-height sheathing as shown in **Figure 1**.

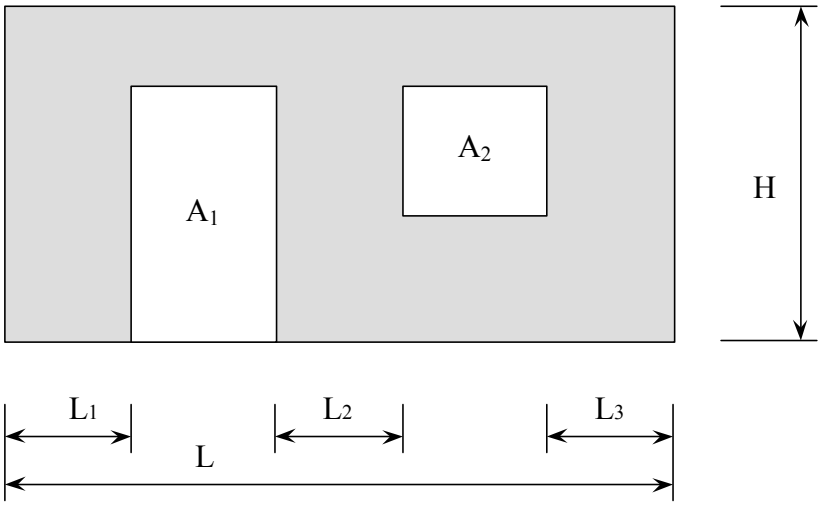

Figure 1 - Sheathing area ratio.

Initially, Yasumura and Sugiyama [21] proposed the following equation for the shear capacity ratio, or the ratio of the strength of a shear wall segment with openings to the strength of a fully sheathed shear wall segment without openings:

$$F = \frac{r}{3 - 2r} \tag{2}$$

The relationship was derived based on results of monotonic racking tests on 1/3-scale walls and was considered applicable for the apparent shear deformation angle of 1/100 radian and for ultimate load. Later, Sugiyama and Matsumoto [20] published two more equations based on tests of longer wall models and suggested for use in North-American wood-frame construction:

$$F = \frac{3r}{8 - 5r} \tag{3}$$

for the shear deformation angle $\gamma = 1/300$ radian, and

$$F = \frac{r}{2 - r} \tag{4}$$

for $\gamma = 1/100$ and $1/60$ radian.

The authors [20] suggest two limitations on the use of Equations (3) and (4):

1) The depth-to-width ratio in the wall space above and/or below an opening is not less than 1/8;
2) The sheathing area ratio is not less than 30%.

Tabulated shear capacity ratios or opening adjustment factors appearing in the SBC and WFCM are based on Equation (2) assuming that the height of all openings in a wall are equal to the largest opening height. The decision to use Equation (2) rather than Equation (3) as the basis of design was made so that the design values would be conservative in all cases. The result is that SBC and WFCM tabulated shear capacity ratios or opening adjustment factors for walls containing openings of varying height are smaller than would be calculated using Equation (2) and, therefore, are more conservative. The WFCM uses a full-height sheathing length adjustment factor in the application of Equation (2) to design. The adjustment factor depends on the maximum opening height in the wall, and is multiplied by the length of wall required if there are no openings present.

Johnson [9] tested 12.2-m (40-ft.) long walls of five configurations with sheathing area ratio varying from 0.3 to 1.0. Wall of each configuration was tested once monotonically and once cyclically. The specimens were constructed in accordance with the requirements of perforated shear wall design method, i.e. tie-down anchors applied at the wall ends. Structural 12-mm (15/32-in.) plywood sheathing was attached on one side and 13-mm (1/2-in.) gypsum wallboard - on the other. Heine [9] tested three of the same configurations monotonically and cyclically with 11-mm (7/16-in.) oriented strandboard (OSB) instead of plywood. Both studies proved

Equation (2) to be conservative in predicting both monotonic and cyclic capacities of long shear walls.

TEST PROGRAM

Five wall configurations tested by Johnson [10] and reported by Dolan and Johnson [5, 6] were used as appropriate configurations in construction of wall specimens for this study. Apart from framing material and connections, the differences from previous tests were as follows:

1) The headers and sheathing was connected to the rest of the wall framing in the weakest possible configuration (i.e., no sheathing gussets around openings, no special strapping, etc.)
2) 11-mm (7/16-in.) OSB sheathing instead of 12-mm (15/32-in.) plywood was used for exterior sheathing (similar to the wood-frame configurations tested by Heine [7]);
3) 13-mm (1/2-in.) gypsum drywall interior sheathing was omitted except for two monotonic tests of fully-sheathed walls (Configuration **A**) (this was done so that the results would more clearly correlate with current code approved shear values, and to ensure the results remained conservative);
4) Instrumented tension bolts were used to measure uplift forces transferred through tie-down anchors at the ends of walls.
5) Specimens were mirror image of walls tested by Johnson [10] i.e. load was applied to the opposite send of the wall. (Load was applied to the left-hand end of the specimens shown in Table 1.) A second change is that the cold-formed steel framed walls had stud spacing at 24 inches on center instead of 16 inches.

Monotonic and cyclic tests were conducted on walls of each configuration shown in **Table 1**. Size and placement of openings were selected to cover the range of sheathing area ratios encountered in light-frame construction. With the exception of two monotonic tests, gypsum sheathing was omitted to provide correlation with design code values (UBC, SBCCI, BOCA, and IBC), test the weakest conditions, and minimize variables in the tests. It is known

from previous experiments [12, 13, 14] that under cyclic loading gypsum wallboard does not add to the shear strength of the wall, while under monotonic loads capacities of various sheathing materials are usually additive. All specimens were built in accordance with the *Builder's Steel-Stud Guide* [3] and framed and sheathed to provide the weakest condition that still conformed to the design specification. For instance, headers over openings were framed as shown in Figure 2 rather than using methods to increase fixity such as extended strapping or blocking.

Figure 2 Typical Header Detail.

Specimen Configuration

All specimens were 12.2-m (40-ft.) long and 2.4-m (8-ft.) tall with the same type of framing, sheathing, fasteners, and fastener schedules. **Table 1** lists the opening dimensions and illustrates the opening locations for each wall configuration. Wall **A** (r = 1.0) had no openings

and was included in the investigation for determining the capacity of the fully sheathed wall. The ratios of strength of Walls **B** through **E** to Wall **A** were compared directly to the shear capacity ratio, F, calculated using Equations (2), (3), and (4).

Table 1 - Wall configurations and opening sizes.

Wall configuration [1, 4, 5]	Wall type	Sheathing area ratio, (r)	Opening size	
			Door	Window [2]
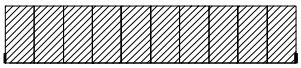	**A**	1.0	-	-
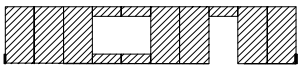	**B**	0.76	6'-8" × 4'-0"	5'-8" × 7'-10½"
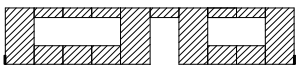	**C**	0.56	6'-8" × 4'-0"	4'-0" × 11'-10½" 4'-0" × 7'-10½"
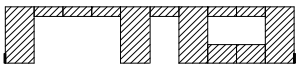	**D**	0.48	6'-8" × 4'-0" 6'-8" × 12'-0"	4'-0" × 7'-10½"
	**E**	0.30	(Sheathed at ends) [3] 8'-0" × 28'-0"	-

1: All walls are framed with studs spaced at 24 inches on center. Shaded areas represent sheathing.
2: The top of each window is located 16 inches from the top of the wall.
3: Wall E has studs along the full length of wall but is sheathed only at the ends of the wall.
4: Load was applied to the top left-hand corner of the specimens in either monotonic racking (compression) or reversed cyclic racking.
5: 5/8 inch anchor bolts with 1-1/2 inch round washers were located at 24 inches o.c. along the top and bottom of the specimen except for pedestrian and garage door openings.
Note: 1ft. = 304.8 mm, 1in. = 25.4 mm

Materials and Fabrication Details

Table 2 summarizes materials and construction details used for the wall specimens. Included are the sizes of headers and jack studs used around openings. Wall framing consisted of single top and bottom tracks, single intermediate and double end-studs, and double studs around doors and windows. All frame members consisted of cold-formed steel profile. Cee--shaped members were used for studs and headers, whereas track was used for top and bottom plates.

Tracks (350T1.25-33) had 89-mm (3.5-in.) width (web) and intermediate studs (350S150-33) were spaced 610 mm (24 in.) on center.

Table 2 - Wall materials and construction data

Component	Fabrication and Materials
Studs Top and bottom tracks	350S150-33 (2×4 Cee-section cold-formed steel stud, 33 mil) 350T125-33(2×4 cold-formed steel track, 33 mil)
Sheathing: Exterior Interior [1]	 OSB, 7/16 in., 4×8 ft. sheets installed vertically. Gypsum wallboard, ½ in., installed vertically, joints taped
Headers: 4'-0" opening 7'-10 1/2" opening 11' - 10 1/2" opening	 (2) 600S163-43 (2 × 6 steel headers, 43 mil. One jack stud at each end.) (2) 1000S163-54 (2 × 10 steel headers, 54 mil. Two jack studs at each end.) (2) 1000S163-54 (2 × 10 steel headers, 54 mil. Two jack studs at each end.)
Tie-down	Simpson HTT 22, fastened to end studs with 32 #8, self-drilling screws; 5/8-in. diameter A307 bolt to connect to foundation.
Shear Bolts	5/8-in. diameter A307 bolts with 1½-in.round washers; 24 in. on center

1: If applied. Note: 1ft. = 304.8 mm, 1in. = 25.4 mm

Exterior sheathing was 11-mm (7/16-in.) OSB. All full-height panels were 1.2×2.4-m (4×8 ft.) and oriented vertically. To accommodate openings, the panels were cut to fit above and below the doors and windows. OSB sheathing was applied with joints located at the ends of headers to simulate the weakest condition possible. Interior sheathing was applied in two additional monotonic tests of walls **A**. It was 13-mm (1/2-in.) gypsum wallboard in 4×8-ft. sheets oriented vertically. All joints in the interior sheathing were taped and covered with drywall compound. Compound drying time complied with the manufacturer's recommendation and was adjusted to ambient temperature and humidity. Specimens were attached to 76×127-mm (3×5-in.) steel tubes at the top and the bottom. The test fixture was narrower than the framing, therefore, both exterior and interior sheathing were able to rotate past the test fixture at the top and bottom.

Two tie-down anchors were used, one at each double stud at the wall ends. For this purpose, a Simpson Tie-down model HTT22 was attached to the bottom of the end studs by

thirty-two #8 self-drilling framing screws with a hex head. A 15.9-mm (5/8-in.) diameter bolt connected the tie-down, through the bottom track, to the structural steel tube test fixture.

Table 3 shows the fastener schedule used in constructing the wall specimens. Three types of screws were used: #8 self-drilling screws with low-profile head connected the framing where sheathing was to be installed, #8 self-drilling screws with hex heads were used otherwise, and #8 self-drilling screws with bugle-heads attached sheathing to the frame. Sheathing screws were spaced 152 mm (6 in.) on perimeter and 305 mm (12 in.) in field to attach OSB sheathing and 178 mm (7 in.) on perimeter and 254 mm (10 in.) in field - for gypsum wallboard. A minimum edge distance of 9.5 mm (3/8 in.) was maintained in all tests. Tie-down anchors were attached to the double end studs using #8 self-drilling screws with hex heads, one located in each of the 32 pre-punched holes in the metal anchor.

Table 3 - Fastener schedule

Connection Description	No. and Type of Connector	Connector Spacing
Framing	Screws:	
Top / Bottom Plate to Stud	2 - #8, self-drilling, low-profile head[1]	per stud at each end
Stud to Stud	#8, self-drilling, hex head[2]	24 in. o.c.
Stud to Header	2 - #8, self-drilling, low-profile head[1]	per stud at each end
Header to Header	#8, self-drilling, hex head[2]	16 in. o.c.
Tie-down Anchor/ Shear Bolts		
Tie-down Anchor to Stud	32 - #8, self-drilling, hex head screws[2]	per tie-down
Tie-down to Foundation	1 - A307 ∅5/8-in. bolt	per tie-down
Shear bolts	1 - A307 ∅5/8-in. bolt with 1½-in. steel washers	24 in. o.c.
Sheathing:		
OSB	#8, self-drilling, bugle-head screws[3]	6 in. edge / 12 in. field (2 rows for end stud)
Gypsum wallboard[4]	#8, self-drilling, bugle-head screws[3]	7 in. edge / 10 in. field

Note: 1ft. = 304.8 mm, 1in. = 25.4 mm

1. Grabber item # 2347, 8 x 1/2 Pan head
2. Grabber item # 10075H3, 10 x 3/4 Hex head
3. Grabber item # P81516F3, 8 x 1 15/16 Bugle head
4. Two (2) Tests with monotonic loading only

Test Setup

Tests were performed with the shear walls in a horizontal position as shown in **Figure 3**, with OSB sheathing on top. The wall was raised 0.41 m (16 in.) above the ground to allow sufficient clearance for instruments and the load cell to be attached to the wall. In this setup, no dead load was applied in the plane of the wall, which conservatively represented walls parallel to floor joists. Racking load was applied to the top right corner of the wall (for the configurations shown in **Table 1**) by a programmable servo-hydraulic actuator with the range of displacement of ±152 mm (6 in.) and capacity of 245 kN (55 Kips). Load was distributed along the length of the wall by means of a 76×127-mm (3×5-in.) steel tube attached to the top plate of the wall with 15.9-mm (5/8-in.) diameter bolts at 610 mm (24 in.) on center. Oversize of bolt holes was limited to 0.8 mm (1/32 in.) to minimize slip. Bolts attaching the bottom plate were located a minimum of 305 mm (12 in.) away from the studs adjacent to openings or end of wall. Although, the *Builder's Steel-Stud Guide* [3] requires a piece of steel stud underlying the nut to serve as a washer, 38-mm (1.5-in.) round washers were used instead to ensure the test results were conservative. Eight casters were attached to the distribution beam parallel to loading to allow free horizontal motion.

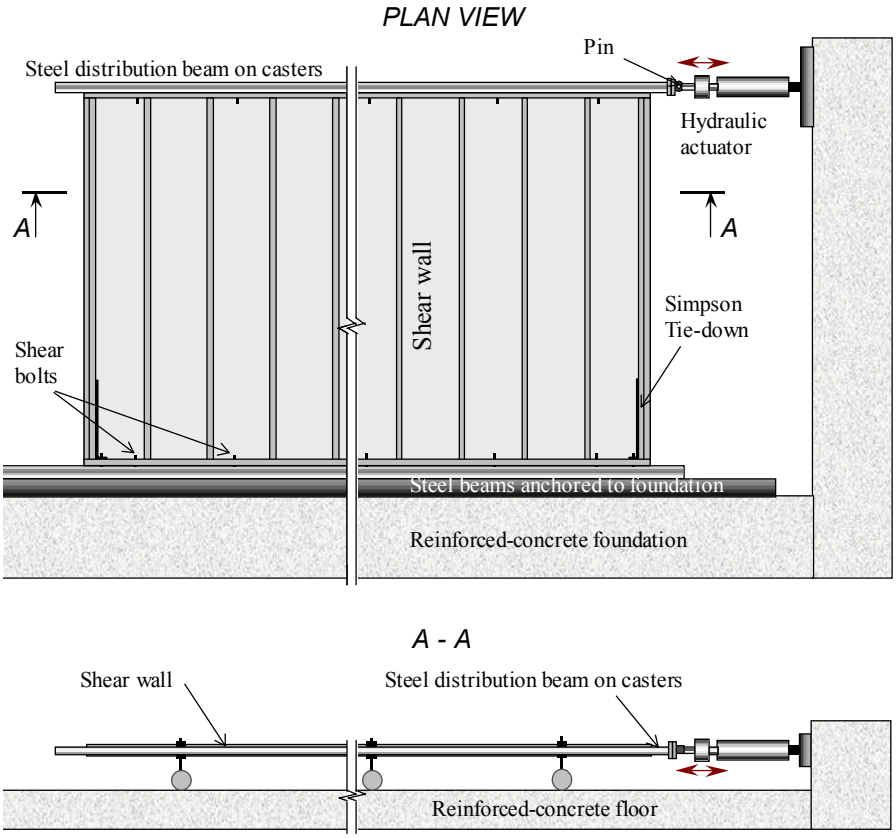

Figure 3 - Test Setup.

Instrumentation and Measurements

Figure 4 shows the data acquisition system used in the tests. The hydraulic actuator contained the load cell (channel #6) and internal LVDT (channel #7) that supplied information on applied force and displacement. In addition, each specimen accommodated two resistance potentiometers (pots), two instrumented bolts, and two linear variable differential transformers (LVDT's).

Bolts (channels #1 and #2) were instrumented with strain gages, which allowed direct measuring of tension forces resisted in the overturning anchors during loading. LVDT's (channels #3 and #4) were mounted on the foundation to measure uplift displacement of the frame. Pots (channels #5 and #8) attached to the foundation measured lateral translation of the top and bottom plates, respectively. The difference between the readings of these two instruments produced story

drift. Pot (channel #8) readings and the difference between readings of LVDT (channel #7) and pot (channel #5) showed the amount of the bottom and top plate slippage along the foundation and the distribution beam, respectively. Data was recorded at a frequency 10 Hz in monotonic tests and 20 Hz in cyclic tests.

Load Regimes

Two load regimes were used in testing the walls: monotonic and cyclic. Monotonic load was applied at the rate of 15 mm/min (0.6 in./min). Without unloading, the deflection progressively increased from zero to 152 mm (6 in.). For cyclic tests, a sequential phased displacement (SPD) procedure, adopted by Structural Engineers Association of Southern California (SEAOSC) [18] was used in this study in order to be consistent with previous tests. However, recent work by Forintek Canada Corporation suggests that a protocol similar to the proposed ISO or ATC24 tests procedures may be more appropriate. The problem with the SPD protocol is that it requires the specimen to resist significantly higher energy inputs than expected during seismic events. This increase in demand results in fatigue failures of fasteners being the failure mechanism for the tests while failures in the field are rarely fatigue related. The ISO and ATC24 test protocols result in failure mechanisms similar to those observed in field investigations.

The SPD loading consisted of two displacement patterns and is illustrated in **Figure 5** and **Figure 6**. The first pattern gradually displaced the wall to its anticipated yield displacement. Elastic behavior of the wall was observed in this part of the test. The second displacement pattern began once the wall had past its anticipated yield displacement (i.e. started inelastic behavior) or first major event (FME). To make results of the cyclic tests compatible with previous tests [14], FME = 2.5 mm (0.1 in.) was used, although in the tests, FME actually occurred at deflections exceeding 5 mm (0.2 in.).

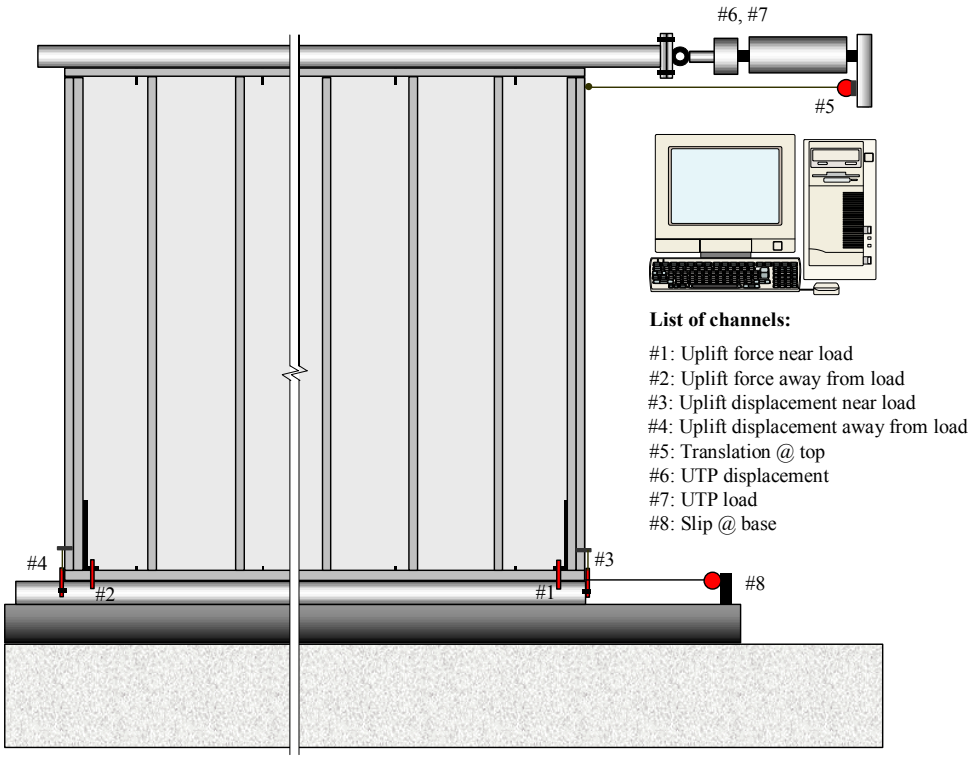

Figure 4 - Data acquisition system.

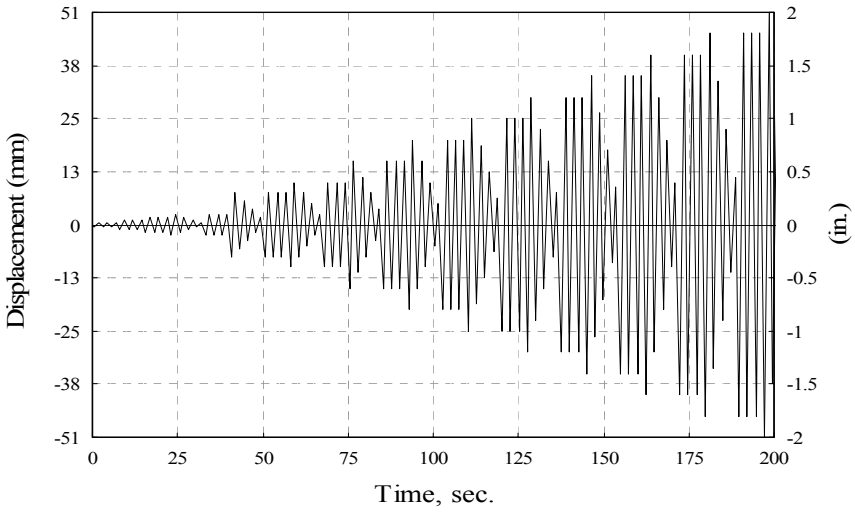

Figure 5 - Displacement pattern of SPD procedure.

The excitation was a triangular reversing ramp function at a frequency of 0.4 Hz. The cycles started with the negative stroke, i.e. with the ram pushing the specimen.

The first displacement pattern consisted of three phases, each containing three full cycles of equal amplitude. The first set of three cycles displaced the wall at approximately 25% of the FME. The second set displaced the wall 50% of the FME and the final set displaced the wall at 75% of the FME. The next cycle displaced the wall to approximately the FME to begin the second displacement pattern.

Figure 6 illustrates one phase of the second displacement pattern in SPD loading. The initial cycle was followed by three decay cycles of 75%, 50%, and 25% of the initial amplitude. The decay cycles were followed by three cycles with the initial amplitude for the phase. Such a pattern was determined to be sufficient in order to obtain a "stabilized" response for nailed shear walls and was found to provide the stabilized response for screws as well. Stabilized response is defined as when the load resistance of the wall at the same amplitude in two successive cycles decreased less than 5%. The amplitude of initial cycle in subsequent phases increased in the following pattern: 200%, 300%, 400%, and so on in 200% increments of the FME displacement until the amplitude reached 102 mm (4 in.).

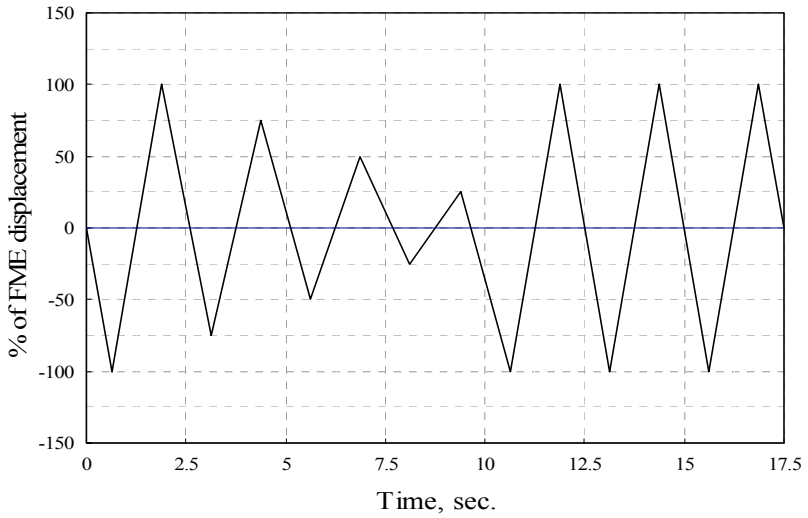

Figure 6 - Single phase of SPD pattern.

PROPERTY DEFINITIONS

Data collected during the wall tests was analyzed using guidelines of SEAOSC [18] and proposed ASTM method [2]. According to these methods, strength, stiffness, and damping characteristics were determined. Definitions of the properties are given in this section.

Story drift was determined as the difference between horizontal movement at the top of the wall (channel #5) and at the bottom plate (channel #8). However, to perform quantitative analyses and comparisons of wall performance, load-deflection curves were generated for each specimen based on data produced by channels #6 and #7 (**Figure 4**). In this case, fewer random and systematic errors related to measurements were involved in computation of wall parameters. On one hand, this allowed obtaining more consistent results and more accurate estimation of energy dissipation. On the other hand, the results conservatively ignored the amount of slip at the top and bottom plates, which varied from 0.1 mm (0.005 in.) at proportional limit to 1 mm (0.04 in.) at peak loads. For analysis of monotonic tests, observed response curves were used. For analysis of cyclic tests, so-called *envelope response curves* were produced.

A typical response curve of shear walls to SPD loading is shown in **Figure 7**. It is a series of hysteresis loops corresponding to each cycle of negative and positive deflections of the wall. From the hysteresis loops, complete (negative and positive) envelope, or 'backbone' curves were determined by producing the line of best fit through the maximum force and associated displacement for each cycle. Two types of envelope curves were obtained. The *'initial' envelope curve* accommodated peak loads from the first cycle of each phase of SPD loading; the *'stabilized' envelope curve* contained peak loads from the last cycle of each phase.

The envelope curves of light-frame shear walls resemble the shape of monotonic response curves. The differences between these curves allow quantifying the strength and stiffness degradation of the structure due to repeated reversed loading. Therefore, all parameters were determined from the three curves: monotonic, initial, and stabilized. The parameters of the

negative and positive envelope curves were averaged assuming variability was due to random effects.

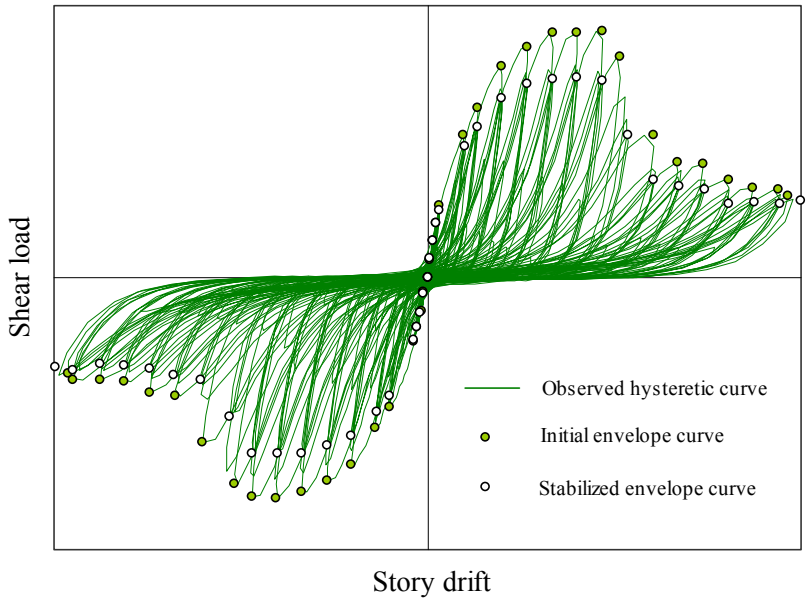

Figure 7 - Typical response curve of a shear wall under SPD loading.

The definitions of variables used in this report are those used for similar investigations of the perforated shear wall method with wood-framed wall specimens. They have not been agreed upon as standard definitions, and there are several other definitions being proposed for many of the variables. However, the variables used provide some measure of performance and the ability to compare performance between specimens. The data can be reanalyzed to provide quantitative information once the variable definitions are finalized.

Figure 8 reveals how strength and stiffness parameters were defined from a load-deflection or envelope curve. Capacity of wall, F_{max}, was determined as the extreme load in the corresponding load-deflection curve. Deflection corresponding to the capacity was determined and denoted as Δ_{peak}. Failure load, $F_{failure}$, and corresponding deflection, $\Delta_{failure}$, were found at the point of significant drop in resistance or when the resistance dropped to 80% of the wall capacity, whichever was greater. In this report, elastic stiffness, k_e, was defined as the slope of the line

passing through the origin and the point on the response curve where the load was equal 40% of F_{max}. This is one of the questionable definitions used in this report. The definition is one that was used in the proposed ASTM standard for cyclic tests of mechanical connections, and is a compromise reached in an effort to harmonize the ASTM test standard and the CEN standard. The variable may need to be adjusted once a final definition is reached. This definition also affects the values determined for other variables that used the initial stiffness directly or indirectly such as ductility. In cyclic tests, this stiffness represented a good estimate of the stiffness that shear walls would exhibit after being loaded a number of times at low to moderate amplitudes.

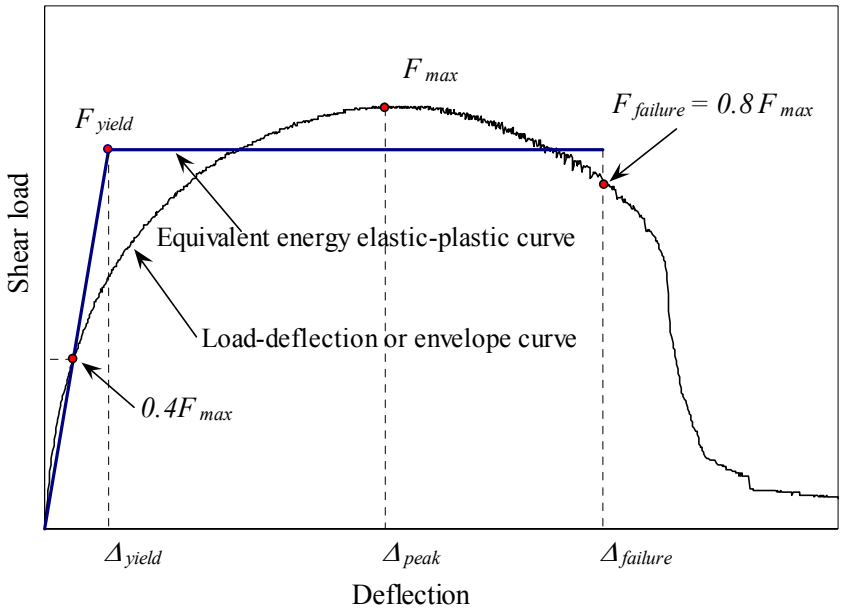

Figure 8 - Performance parameters of shear walls.

For comparison purposes, an equivalent energy elastic-plastic (EEEP) curve was determined for each wall. This artificial curve, shown in **Figure 8**, depicts how an ideal perfectly elastic-plastic wall would perform and dissipate an equivalent amount of energy. This definition of the EEEP curve was used for both monotonic and cyclic tests.[1)]

[1)] Total energy dissipated by walls during cyclic tests is significantly greater than determined from the envelope curve because hysteresis loops overlap. This definition is used for comparison purposes only.

The elastic portion of the EEEP curve contains the origin and has a slope equal to the elastic stiffness, k_e. The plastic portion of the EEEP curve is a horizontal line positioned so that the area under the EEEP curve equals the area under the response curve from zero deflection to $\Delta_{failure}$. Displacement at yield, Δ_{yield}, and load at yield, F_{yield}, are defined at the intersection point of the elastic and plastic lines of the EEEP curve.[2)] Equating the areas under the response curve and the EEEP curve, the yield load can be expressed [7]:

$$F_{yield} = \frac{-\Delta_{failure} \pm \sqrt{\Delta_{failure}^2 - \frac{2A}{k_e}}}{-\frac{1}{k_e}} \tag{5}$$

where: A = area under the response curve between zero and $\Delta_{failure}$.

Information about deformation of walls is an important parameter that indicates the ability to sustain relatively high loads at significant deflections. Useful information about wall deformation capacity is provided by ductility ratio, D, and so-called toughness of failure, D_f, determined from the EEEP curve:

$$D = \Delta_{failure} / \Delta_{yield} \tag{6}$$

$$D_f = \Delta_{failure} / \Delta_{peak} \tag{7}$$

Another important characteristic of cyclic performance of structural systems is their ability to dissipate the strain energy, or damping. Damping energy, W_D, dissipated per cycle y the wall is calculated by integrating the area enclosed by the hysteresis loop at the corresponding displacement (as shown in **Figure 9**). The strain energy, U_0, equals the area enclosed by the triangle *ABC* in **Figure 9**. To compare damping properties of the walls, equivalent viscous damping ratio for each initial and stabilized cycle, ζ_{eq}, and work to failure were estimated:

[2)] F_{yield} must be greater than or equal to 80% of F_{max}.

$$\zeta_{eq} = \frac{1}{4\pi}\frac{W_D}{U_0} \tag{8}$$

Since hysteresis loops were not ideally symmetric, the areas of triangles *ABC* and *ADE* in **Figure 9** were averaged to approximate the value of the strain energy U_0 in Equation (8).

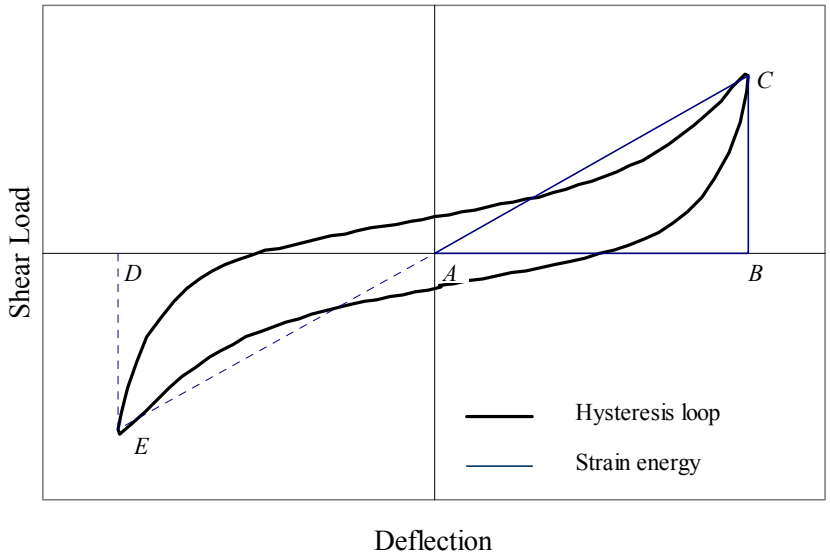

Figure 9 - Damping and strain energy of a cycle.

Work to failure, or energy dissipation, was measured as the total area enclosed by hysteresis loops until failure in cyclic tests, or the area under the load-deflection curve until failure in monotonic tests.

To validate Equations (2) to (4), load resisted by walls at shear angles 1/300, 1/200, 1/100, and 1/60 radian were extracted from the monotonic, cyclic initial and stabilized data. These angles correspond to deflections of 8 mm (0.32 in.), 12 mm (0.48 in.), 24 mm (0.96 in.), and 41 mm (1.6 in.). To determine actual shear capacity ratio at a given deflection, the load resisted by a wall with sheathing area ratio *r* was divided by the corresponding load resisted by the fully sheathed wall.

In addition to the parameters introduced in this section, the discussion of test results includes uplift forces resisted by tie-down anchors, uplift movement of end studs, failure modes, and general observations.

TEST RESULTS

A total of 17 specimens were constructed and tested in this study. The number of tests performed in each category and their basic nomenclature (in bold characters) are displayed in **Table 4**. **Appendix A** contains summary data for each specimen tested including parameters defined in the previous section. **Appendix B** contains observed load-deflection curves along with graphs of uplift forces and displacements at the wall ends as a function of wall deflection. Note that load-deflection curves in **Figures 10** and **11** in this section were plotted using reduced data for convenience of display. Graphs in **Appendix B** display original non-reduced data.

Table 4 - Number of tests.

Load regime	Wall type						
	Agyp [1]	**A**	**B**	**C**	**D**	**E**	Total
monotonic	1	1	1	1	1	1	6
cyclic	-	2	2	2	2	2	10
Total	1	3	3	3	3	3	16

1: These walls had interior gypsum wallboard sheathing in addition to exterior OSB sheathing.

One monotonic and two cyclic tests were performed on each wall configuration. Walls **Agyp** were tested monotonically to isolate the effect of gypsum sheathing and to acquire a reference point for quantifying opening size effects. As shown in **Figure 12**, fully sheathed walls developed significantly different capacities and corresponding deflections in the monotonic tests depending on whether gypsum was applied or not. For opening effects, specimen **Amon** was used as a control trial for all other wall configurations.

Effects of opening size

To illustrate response of walls with various opening sizes, **Figure 10** shows load-deflection and envelope curves observed in monotonic and cyclic tests, and Table 5 summarizes performance parameters obtained from the analysis of these curves. Note that the data are based on single replications for monotonic tests and on two replications for cyclic tests. Each envelope curve represents the average of negative and positive envelopes of individual specimens. Both replications are shown in the graphs to illustrate variation in the cyclic response of walls. Cyclic data in Table 5 represent average values of two specimens, which in turn were obtained by averaging parameters determined separately for negative and positive envelopes.

Table 5 - Performance parameters of walls with various openings.

Parameter	Load condition	Units	Wall configuration				
			A	**B**	**C**	**D**	**E**
F_{max}	*monotonic*	*Kips*	32.5	20.7	13.9	12.8	7.7
	cyclic initial		26.7	20.5	13.3	11.6	6.5
	cyclic stabilized		21.7	17.5	11.7	10.1	5.6
Δ_{peak}	*monotonic*	*in.*	1.49	2.19	2.09	1.84	2.85
	cyclic initial		1.31	1.41	1.49	1.51	1.66
	cyclic stabilized		1.16	1.30	1.46	1.46	1.50
F_{yield}	*monotonic*	*Kips*	28.1	18.5	12.6	11.6	6.7
	cyclic initial		24.1	18.2	11.8	10.3	5.7
	cyclic stabilized		19.6	15.5	10.3	9.0	4.9
Δ_{yield}	*monotonic*	*in.*	0.41	0.46	0.54	0.76	0.82
	cyclic initial		0.38	0.54	0.54	0.56	0.58
	cyclic stabilized		0.30	0.47	0.49	0.51	0.51
$\Delta_{failure}$	*monotonic*	*in.*	2.05	2.55	2.44	2.51	4.31
	cyclic initial		1.68	1.90	2.43	2.37	2.07
	cyclic stabilized		1.58	1.75	2.20	2.39	1.93
k_e	*monotonic*	*Kip/in.*	68.4	40.5	23.4	15.3	8.3
	cyclic initial		64.1	33.7	21.9	18.5	9.8
	cyclic stabilized		66.7	33.1	21.1	18.0	9.6
ζ_{eq} [1]	*cyclic initial*		0.079	0.076	0.070	0.073	0.068
	cyclic stabilized		0.059	0.060	0.056	0.059	0.052

1: ζ_{eq} at F_{max}
Note: 1Kip = 4.448 kN, 1in. = 25.4 mm.

a)

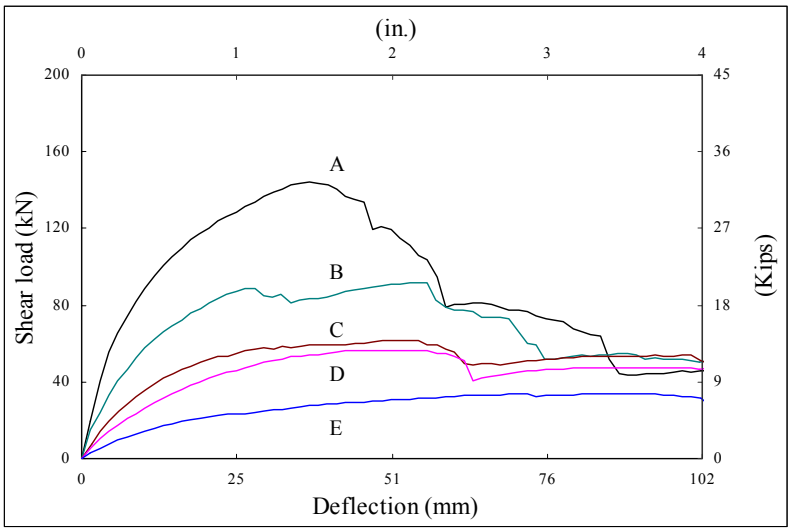

b)

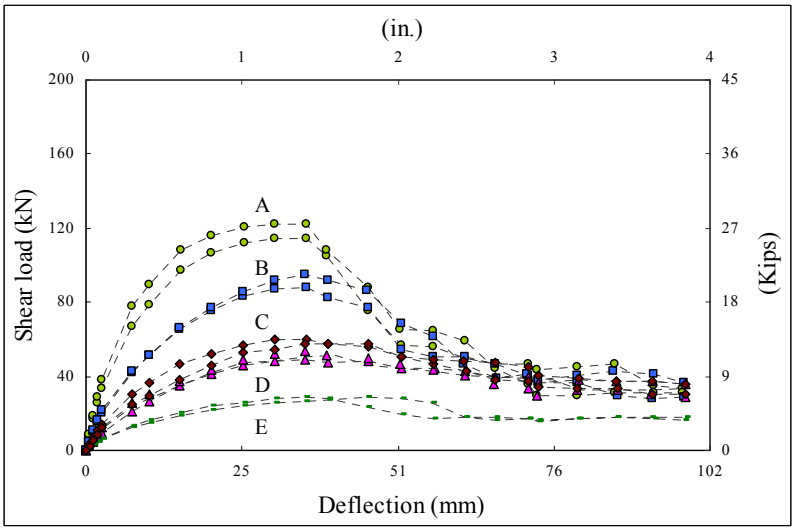

c)

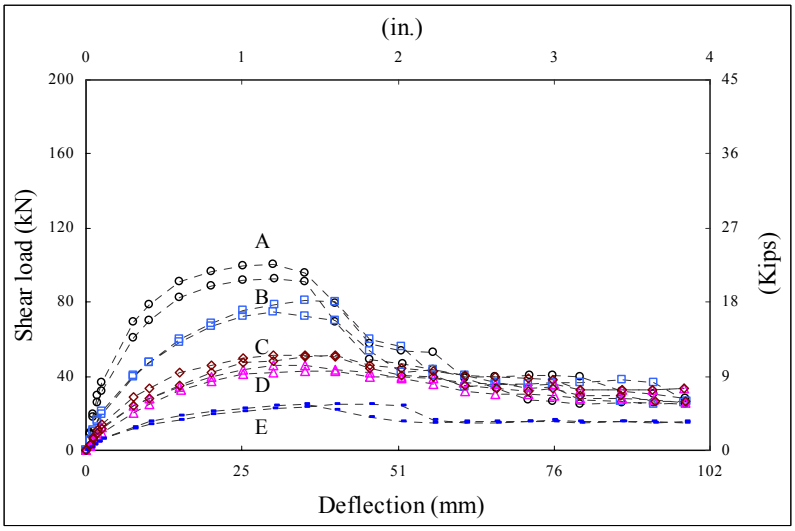

Figure 10 - Response of walls with various openings:

a) monotonic load-deflection curves, b) initial envelope curves, c) stabilized envelope curves.

Effects of opening size on load resistance of each specimen at various levels of deflection under monotonic and cyclic loading are illustrated in **Figure 11**. In the graphs, shear load ratio is shown as a function of sheathing area ratio. Lines represent predictions of shear load ratios given by Equations (2), (3), and (4). **Table 6** provides numerical support for the graphs. Cyclic data in the table is represented by average values of two specimens.

Results suggest that Equation (2) (used in the design codes to determine shear wall strength) and Equation (3) produced overly conservative estimates. At all levels of deflection under monotonic and cyclic loading, the resistance of each specimen significantly exceeded values predicted by these equations. For both load regimes, the closest predictions were obtained at the early stages of deflection using Equation (4). The shear load ratios at 8 mm (0.32 in.) and 12 mm (0.48 in.) deflections were predicted with ±15% accuracy. With transition to higher deflection levels, the estimates of Equation (4) also became conservative and increased in conservatism with cycling at amplitudes beyond yield point.

Table 6 - Predicted and observed shear load ratio

Shear load ratio	Load condition	Wall configuration			
		B	**C**	**D**	**E**
Predicted	$F = 3r/(8-5r)$ (Eq. 3)	0.541	0.320	0.257	0.138
	$F = r/(3-2r)$ (Eq. 2)	0.512	0.295	0.235	0.125
	$F = r/(2-r)$ (Eq. 4)	0.612	0.386	0.316	0.176
F @ 0.32 in.	*monotonic*	0.633	0.393	0.283	0.157
	cyclic initial	0.596	0.387	0.330	0.178
	cyclic stabilized	0.619	0.402	0.344	0.187
F @ 0.48 in.	*monotonic*	0.658	0.412	0.307	0.169
	cyclic initial	0.625	0.402	0.347	0.188
	cyclic stabilized	0.655	0.426	0.366	0.200
F @ 0.96 in.	*monotonic*	0.680	0.423	0.361	0.182
	cyclic initial	0.716	0.465	0.402	0.213
	cyclic stabilized	0.763	0.501	0.438	0.229
F @ 1.60 in.	*monotonic*	0.600	0.420	0.392	0.201
	cyclic initial	0.848	0.567	0.488	0.269
	cyclic stabilized	0.997	0.679	0.580	0.314
$F @ \Delta_{max}$	*monotonic*	0.637	0.426	0.394	0.236
	cyclic initial	0.768	0.498	0.434	0.242
	cyclic stabilized	0.807	0.539	0.468	0.259

Note: 1in. = 25.4 mm.

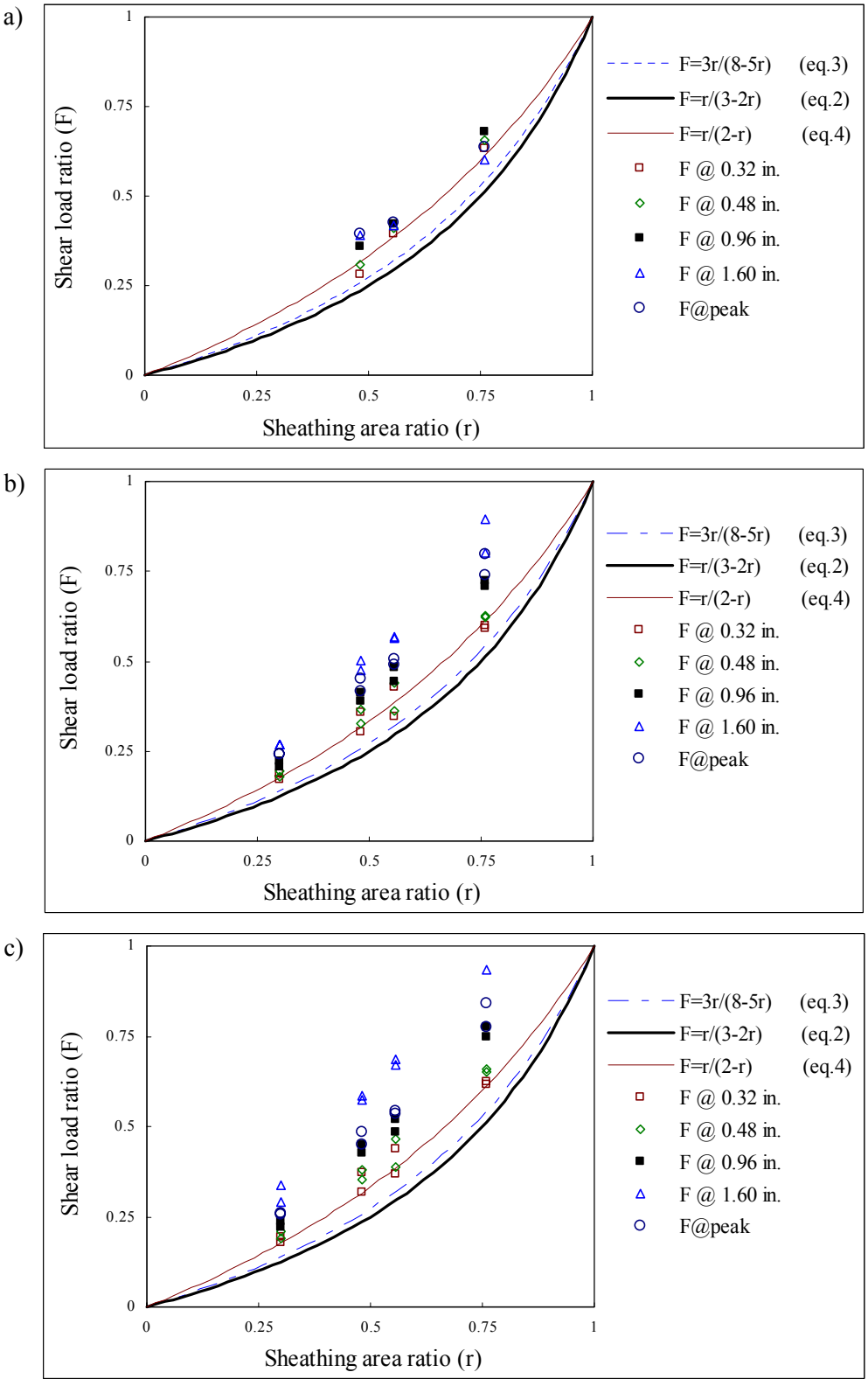

Figure 11 - Shear load ratios:

a) monotonic response, b) initial cyclic response, b) stabilized cyclic response.

The reasons for obtaining so high shear load ratios can be found by looking at Tables 5 and 6. Although fully sheathed walls (**A**) were significantly stiffer than walls with openings, they were also less ductile. Walls **A** reached capacity and degraded earlier than other walls, especially in cyclic tests. This behavior is similar to wood frame wall performance. Wall configuration A is a fully engineered wall configuration with full overturning restraint, while all other configurations are partially restrained. A similar trend was characteristic of wood-frame walls tested by Johnson [10] and Heine [7].

Comparisons of elastic stiffness and yield points in Tables 5 and 6 indicate that walls with larger openings were less stiff under both monotonic and cyclic load conditions. This is why these wall have higher displacement capability.

Effects of cyclic loading

To investigate effects of cyclic loading on performance of steel-frame walls, the data in Tables 5 and **6** were normalized as follows. To compare monotonic and cyclic response, cyclic parameters were related to corresponding monotonic criteria. To estimate effect of repeated cycling, stabilized cyclic parameters were normalized to initial cyclic data. The results are displayed in **Table 7**.

Generally, elastic performance of walls under cyclic loading was comparable to that under monotonic regime despite high variation. Elastic stiffness deviated in both directions approximately ±20%. Major differences took place in the yield zone. Various performance parameters were influenced to a different degree depending on the wall configuration. In comparison with other parameters, cyclic loading affected wall deflections at peak load most of all. Stabilized cyclic capacity developed at 32% to 47% smaller deflections than in the corresponding monotonic tests. Most sensitive to cyclic loading were walls **A** and **E**. Cyclic response of intermediate wall configurations was least influenced. Initial cyclic capacities of walls **A** and **E** were 16% to 18% smaller than the monotonic values, while the corresponding

parameters of walls **B**, **C**, and **D** decreased less than 10%. Although, $\Delta_{failure}$ varied in a wide range, it was up to 50% smaller in cyclic tests than monotonic tests. The decrease in displacements is similar in magnitude to those observed for wood-framed walls [6].

Table 7 - Normalized performance parameters of walls with various openings.

Parameter	Load condition	Wall configuration				
		A	**B**	**C**	**D**	**E**
F_{max}	*initial / monotonic*	82%	99%	96%	90%	84%
	stabilized / monotonic	67%	84%	84%	79%	73%
	stabilized / initial	81%	85%	88%	87%	87%
Δ_{peak}	*initial / monotonic*	88%	64%	72%	82%	58%
	stabilized / monotonic	78%	60%	70%	79%	53%
	stabilized / initial	88%	92%	97%	97%	91%
F_{yield}	*initial / monotonic*	86%	98%	93%	89%	84%
	stabilized / monotonic	70%	84%	82%	78%	73%
	stabilized / initial	81%	85%	87%	87%	87%
Δ_{yield}	*initial / monotonic*	92%	118%	101%	75%	71%
	stabilized / monotonic	72%	103%	91%	67%	63%
	stabilized / initial	78%	87%	90%	90%	89%
$\Delta_{failure}$	*initial / monotonic*	82%	75%	100%	94%	48%
	stabilized / monotonic	77%	69%	90%	95%	45%
	stabilized / initial	94%	92%	91%	101%	93%
k_e	*initial / monotonic*	94%	83%	94%	121%	119%
	stabilized / monotonic	98%	82%	90%	117%	116%
	stabilized / initial	104%	98%	96%	97%	98%
ζ_{eq} [1]	*stabilized / initial*	74%	78%	80%	81%	77%

1: ζ_{eq} at F_{max}

Stabilized resistance of walls was affected to a greater extent than initial. Relative to initial values, stabilized capacity and yield load were 19% lower for walls **A** and 13% to 15% lower for all other walls. As a result, stabilized strength of walls was up to 33% less than in monotonic tests. Stabilized deformation parameters and elastic stiffness were generally similar to initial response parameters because major events took place in the same phase of excitation, i.e. at the same amplitude. Equivalent viscous damping ratio in stabilized cycles was consistently 19% to 26% lower relative to initial cycle values. Reduced deflections for cyclic performance are

similar in magnitude to those observed by Dolan and Johnson [6] for wood-framed walls. Equivalent values of energy dissipation have not been calculated for wood-framed walls.

One reason for the early failure of walls in cyclic tests was due to extreme energy demands imposed by the SPD procedure. **Table 8** gives comparison of energy dissipated by walls until failure during monotonic and cyclic tests. As a rule, it took more than 100 cycles and more than 8 times the energy of monotonic test to destroy a wall in cyclic tests.

These concerns about the SPD test protocol have been reported by Karacabeyli and Ceccotti [11]. The SPD test protocol requires the connections and assembly to resist 3 – 5 times as much energy input as typically experienced in seismic events. In wood-framed walls, this increased energy demand results in a change in failure mechanism from nail pull out and nail head pull through to nail fatigue. Several discussions are currently underway to change the cyclic test protocol from the SPD to either the International Standards Organization or SAC (SAC joint venture as funded by FEMA) test protocols.

The severity of the SPD protocol manifests itself in steel-frame shear walls by excessive damage to the OSB sheathing around the screw head. Some of the damage may have been minimized, or the effect of the damage minimized if screws with a larger and different shaped head were used. The small bugle head of the screws used pulled through the sheathing. A larger head would have increased the resistance to screw head pull through and associated higher shear wall capacity.

Table 8 - Energy dissipated by walls until failure (Kip·ft.).

Load condition	Wall configuration				
	A	**B**	**C**	**D**	**E**
monotonic	4.3	3.6	2.3	2.1	2.2
cyclic	32.0	30.5	31.0	19.7	10.1
cyclic / monotonic	740%	853%	1365%	956%	463%

Note: 1Kip = 4.448 kN, 1ft. = 0.3048 m.

Effects of gypsum sheathing and steel framing

Performance parameters of walls with (**Amongyp**) and without (**Amon**) gypsum wallboard sheathing under monotonic loading are shown in Table 9. Along with the values, included in the table are comparisons between the walls. Based on these data, it can be concluded that elastic stiffness and strength of walls increased approximately 39% when gypsum sheathing was applied. Deflections at peak loads could not be considered significantly different. Note however, that walls of both types consistently failed immediately after deflection exceeded 52 mm (2 in.) and had similar ductility ratios. Based on monotonic tests of wood-frame fully sheathed walls, other researchers [12, 15] supported the conclusion about the additive strength of gypsum wallboard and structural sheathing. Results reported by Serrette, et al. [15] and these results indicate that the effect of adding gypsum wallboard is similar, and the capacities are additive for monotonic loading.

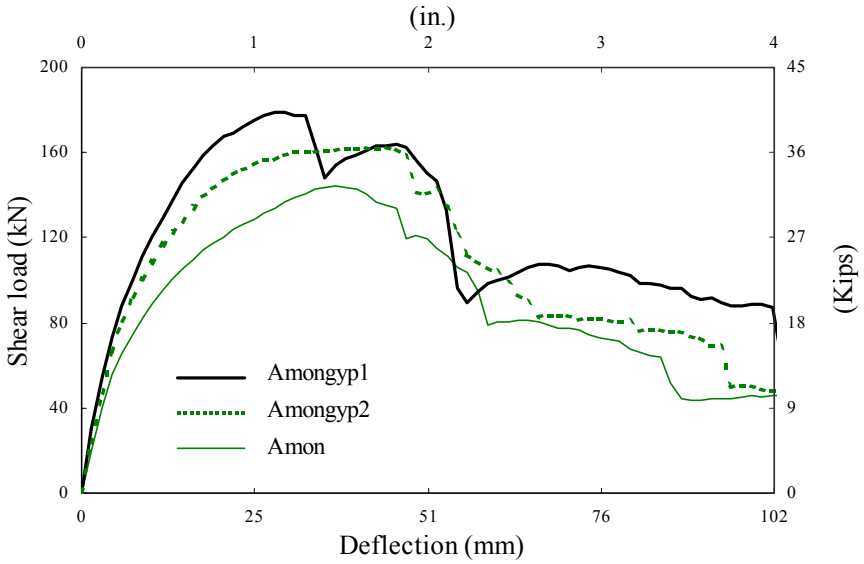

Figure 12 - Monotonic load-deflection curves of walls **A** with and without gypsum sheathing.

General observations

Note on **Figure 12** that the monotonic curves of steel-frame walls descend in a stepwise manner after capacity is exceeded. These steps might be due to the fact that the load increased until edges of adjacent panels bore against each other. The load dropped as soon as the row of fasteners along one of the edges failed entirely and the sheathing overlapped, causing a sudden loss in resistance. This effect is illustrated in **Figure 13**.

Table 9 - Performance parameters of walls with and without gypsum sheathing.

Parameter	Units	**Amon**	**Amongyp**	**Amongyp / Amon**
F_{max}	*Kips*	32.5	40.3	124%
Δ_{peak}	*in.*	1.49	1.16	78%
F_{yield}	*Kips*	28.1	35.5	126%
Δ_{yield}	*in.*	0.41	0.37	90%
Δ@ $0.4F_{max}$	*in.*	0.19	0.17	89%
$\Delta_{failure}$	*in.*	2.05	2.06	100%
k_e	*Kip/in.*	68.4	94.9	139%
W	*Kip ft.*	4.3	5.5	128%
F@ 0.32 in.	*Kips*	17.6	23.6	134%
F@ 0.48 in.	*Kips*	21.6	29.3	136%
F@ 0.96 in.	*Kips*	28.6	39.0	136%
F@ 1.60 in.	*Kips*	31.8	35.9	113%
D		5.0	5.5	110%

Note: 1Kip = 4.448 kN, 1in. = 25.4 mm.

a) b)

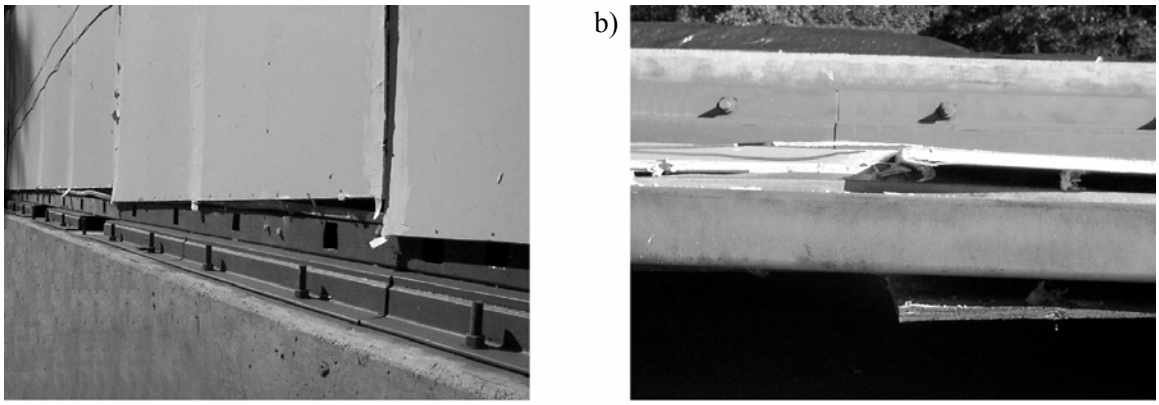

Figure 13 - Failure of wall **Amongyp1**: a) view at the bottom plate, b) view from the top plate.

Steel frames were assembled in the same way they are constructed in buildings. This allowed their racking without separation of studs from the tracks due to pivoting of the stud ends around framing screws. Such assembly was relatively stiff because it engaged all sheathing screws and panel edges into load resistance. The deflection demand on the sheathing connections increased until screws tore through the edge of the sheathing or pulled heads through the sheathing panel as illustrated in **Figure 14**.

a) b)

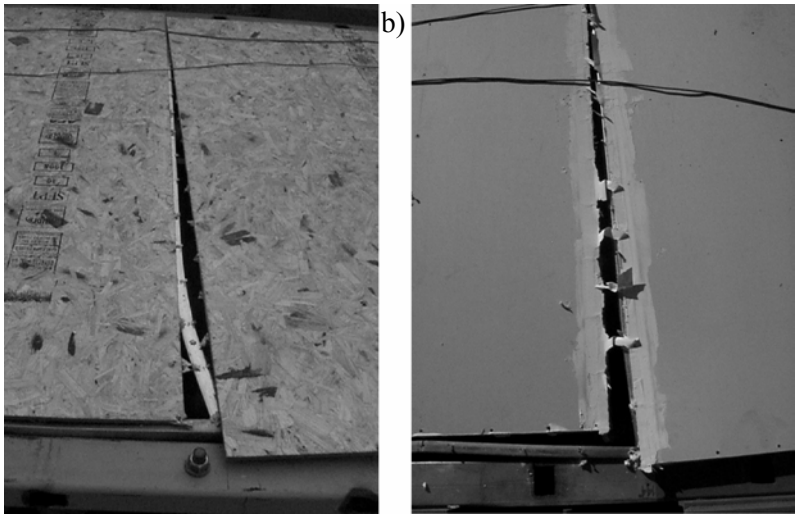

Figure 14 - Unzipped sheathing along the panel edges: a) OSB, b) gypsum wallboard.

While framing connections of steel-frame walls proved to be strong, the framing elements suffered from low bending rigidity. **Figure 15** shows that tracks experienced significant bending especially at the wall ends, which lead to severe damage of sheathing connections.

a) b)

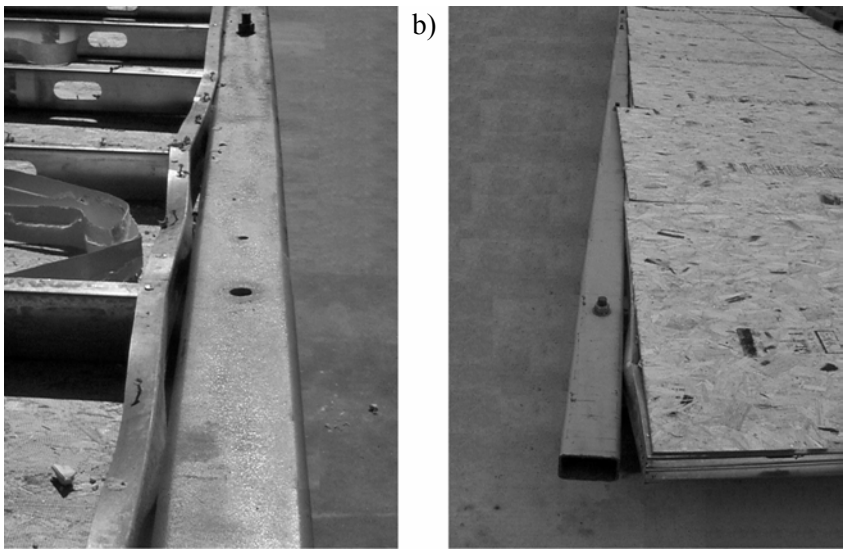

Figure 15 - Bending of top plates: a) wall **Amongyp1**, b) wall **Amon**.

The more sheathing a wall had, the more bending demand was applied to the studs by adjacent panel connections, which resulted in buckling of the studs. **Figure 16** shows the frames of fully sheathed walls after the tests. Note that buckling occurred in the vicinity of openings in the web of the studs due to the reduced section of the stud at these locations.

a) b)

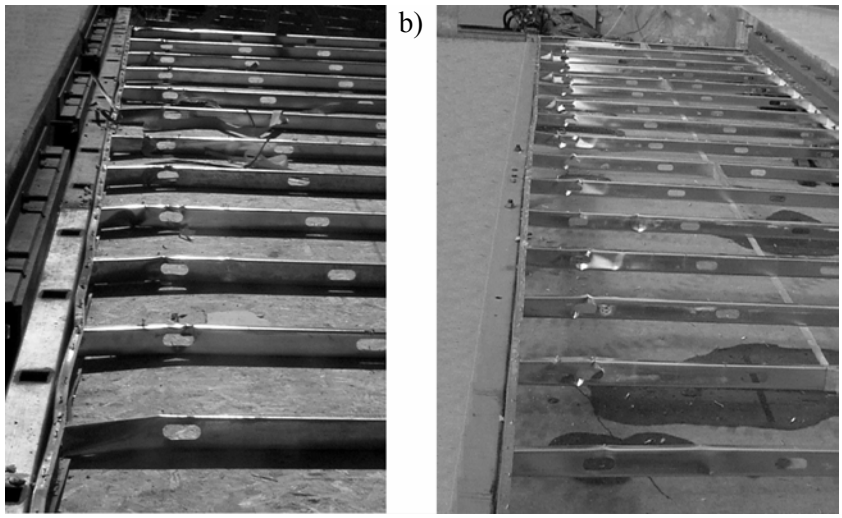

Figure 16 - Buckling of studs in monotonic tests of fully sheathed walls:
a) wall **Amongyp1**, b) wall **Amon**.

End studs in steel-frames developed downward movement due to crushing of the stud material. As illustrated in **Figure 17**, the framing profile was wider than the supporting beam (to ensure free movement of sheathing) allowing local buckling of light-gage steel in compression.

The damage developed early in the test and increased deflection demands on sheathing connections along the top and bottom plates. As shown in the next section and can be seen in **Figure 17**, the local buckling had significant effect at the wall ends in monotonic tests. Intermediate studs were just slightly damaged at the ends as shown in **Figure 18**. The localized crushing of the ends of the studs would be minimized in normal platform construction due to the more uniform loading across the end of the stud when bearing on the platform.

a) b)

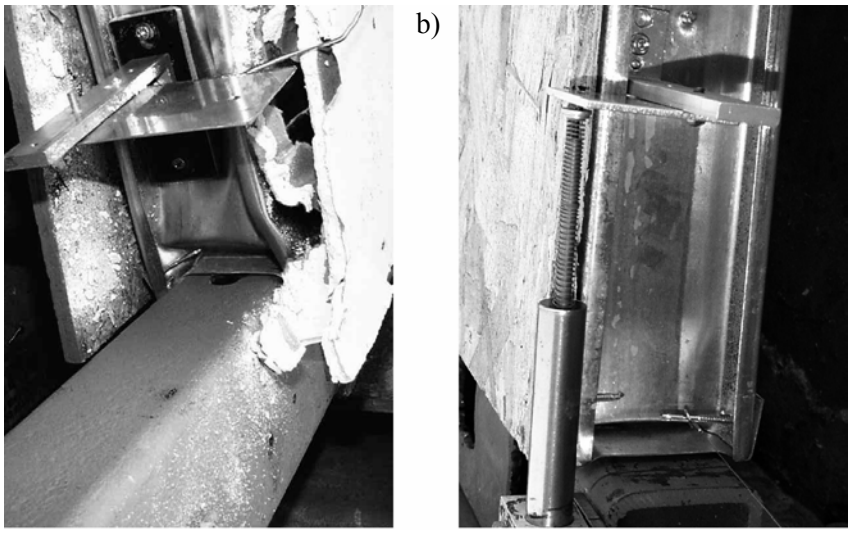

Figure 17 - Local buckling of framing: a) monotonic test (left end), b) cyclic test (right end).

a) b)

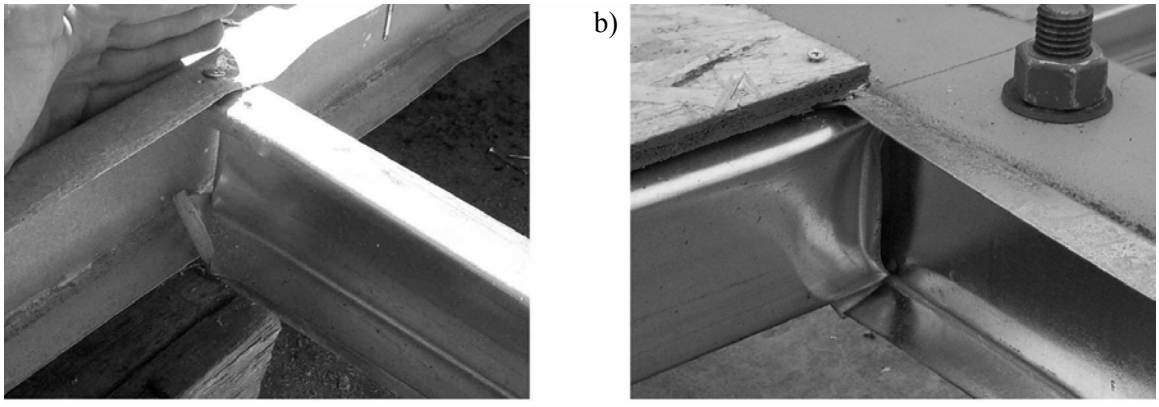

Figure 18 - Local damage of intermediate studs: a) flanges, b) web.

In steel-frame walls, flanges of light-gage profile serve as main members holding sheathing screws in a way that makes them work by pivoting in the flanges to a large extent. The resistance of such pinned connections is governed by the ability of side members (sheathing) to

hold the screw heads. **Figure 19** shows typical failure modes of sheathing connections. Using larger screw heads would probably result in significantly higher stiffness and strength.

a) b)

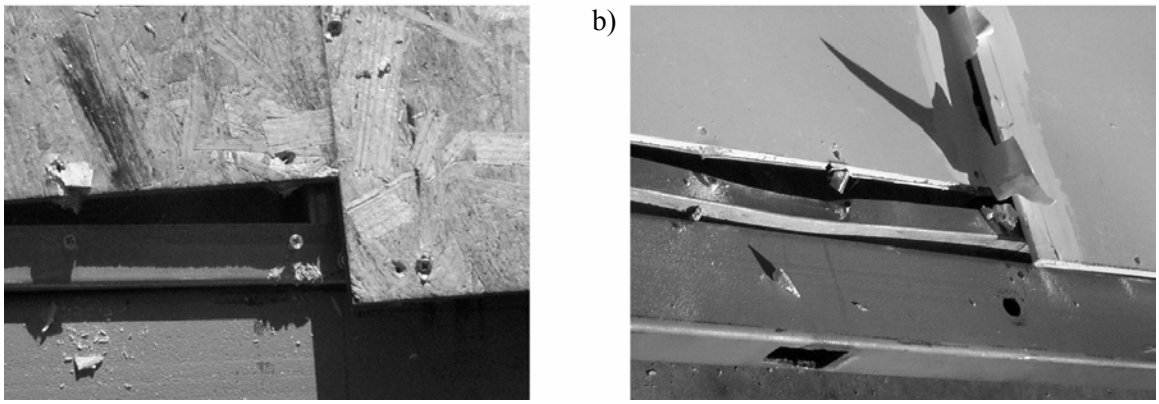

Figure 19 - Typical failure modes of sheathing connections: a) OSB, b) gypsum wallboard.

The predominant failure mode of steel-frame walls was head pull-through of sheathing screws and bending of frame elements. Due to pivoting in the light-gage steel studs, very few screws failed in fatigue. None of the framing screws failed, which kept the framing connections essentially intact (except for crushing at the stud ends). For this reason, the height of the wall remained relatively constant throughout the test and allowed symmetrical pivoting of sheathing panels with arbitrary 'unzipping' of sheathing connections along either top or bottom plates, as well as along studs. This indicates that the sheathing screws had load distributed to them in a fairly uniform manner.

Supplementary measurements

Table 10 summarizes supplementary measurements such as slip of the bottom plate along the platform (*Slip*), vertical movement of end studs (*Right stud* and *Left stud*), and tension force in tie-down bolts (*Tension bolt*). The table gives the values measured in monotonic tests at proportional limit (0.4 @ F_{max}), at capacity (@ F_{max}), and at failure load (@ $F_{failure}$). Also, the

table includes the initial and maximum forces recorded by the tension bolts. Full information on these measurements is shown in individual graphs presented in **Appendix B**.

Maximum slip between the bottom track and the platform was approximately 1 mm (0.04 in.) in all tests because 12 to 20 bolts installed into pre-punched holes prevented slack in the connection between the track and test fixture. Random readings in the slip measurements were caused by end stud movement and the systematic electronic noise was due to low resolution of the potentiometer relative to small magnitudes of change in the measured displacement. As described earlier, due to the small magnitude, the slip between the track and the test fixture was neglected in the evaluation of wall performance parameters to improve precision of calculations. This is conservative in that the effect of the slip is to increase deflections for any given load.

Measurements of vertical movement of end studs supported the observations made earlier. While the uplift movement at one end generally did not exceed 5 mm (0.2 in.), the downward movement at the opposite end was 3 to 4 times larger. The reasons are explained in the previous section.

Tension force in anchor bolts reached maximum at displacements between wall capacity or failure load was reached, depending on the pattern of wall failure. If the end panel containing the load bolt failed first, the tension force in the bolt decreased significantly (wall configurations C and D of Table 10); if the failure started in any other panel, the tension in the bolt sustained the load until the wall completely failed. Although initial tension applied to the bolts at the installation varied between 9 and 22 kN (2 and 5 Kips), the average tension force for walls without gypsum wallboard at wall capacity reached 30 kN (7 Kips) with 8% variation. Note in **Appendix A,** walls with gypsum wallboard developed maximum tension force of 36 kN (8 Kips).

In cyclic tests of steel-frame walls, the amount of slip, vertical movement of studs, and forces in tie-down bolts were comparable to those observed in monotonic tests. The only difference from the monotonic results was due to the fact that the end studs experienced reversed

tension and compression. The magnitude of the uplift displacement at peak loads was on average less than 3 mm (0.1 in.) and twice as much in downward direction.

Table 10 - Supplementary measurements in monotonic tests.

Parameter	Load condition	Units	Wall configuration				
			A	**B**	**C**	**D**	**E**
Slip	@ $0.4F_{max}$	*in.*	0.000	-0.028	0.005	0.005	0.006
	@ F_{max}		0.031	0.031	0.039	0.036	0.031
	@ $F_{failure}$		0.037	0.003	0.035	0.034	0.044
Right stud	@ $0.4F_{max}$	*in.*	0.016	0.031	0.041	0.032	0.008
	@ F_{max}		0.138	0.132	0.436	0.199	0.162
	@ $F_{failure}$		0.166	0.145	0.409	0.170	0.235
Left stud	@ $0.4F_{max}$	*in.*	-0.033	-0.029	-0.040	-0.019	-0.030
	@ F_{max}		-0.422	-0.495	-0.271	-0.141	-0.666
	@ $F_{failure}$		-0.534	-0.493	-0.347	-0.258	-0.934
Tension bolt	*Initial tension*	*lbs*	4493	4923	4733	2068	3657
	@ $0.4F_{max}$		4855	5085	5403	3271	4214
	@ F_{max}		7495	5843	7016	6991	6473
	@ $F_{failure}$		7500	5867	1809	1486	5344
	Maximum tension		7740	5989	7916	7080	6630

Note: 1Kip = 4.448 kN, 1in. = 25.4 mm.

CONCLUSIONS

Based on results of sixteen monotonic and cyclic tests of 12-m (40-ft.) long steel-frame shear walls with and without openings, the following conclusions were made:

1) Comparison of steel-frame wall resistance with predictions of perforated shear wall method and Sugiyama's equations revealed conservative nature of the predictions at all levels of monotonic and cyclic loading. With capacity of 12-m (40-ft.) fully sheathed wall taken as a reference, Equation (4) produced the closest estimates in the elastic range. However, the use of Equation (2), as used in the building codes, is more conservative and will provide acceptable prediction of shear wall strength for both monotonic and cyclic loading in cold-formed steel shear walls.
2) Long, fully-sheathed walls were significantly stiffer and stronger but less ductile than walls with openings. This is due to the increased rocking of wall sections in the middle of the wall specimen that were not restrained against overturning.
3) Cyclic loading did not affect elastic performance of the walls but reduced their deformation capacity ($\Delta_{failure}$). Similar reductions in displacement capacity were observed for equivalent tests for wood-framed walls.
4) Stabilized cyclic strength of walls was up to 19% less than initial cyclic and up to 33% less than monotonic capacities. Strength of fully sheathed walls was affected by cyclic loading to a greater extent than walls with openings. Similar results were observed by Dolan and Johnson [6] for wood-framed walls.
5) In monotonic tests, elastic stiffness and strength of fully sheathed walls increased approximately 39% and 24%, respectively, when gypsum sheathing was applied and the fastener schedules are spaced at 6 inches for the OSB sheathing. The contribution was likely due to full-height taped wallboard seams. Therefore, increase in capacity due to gypsum wallboard sheathing in steel-frame walls with minimum taped joints may be less. The

increase may also be different if the OSB sheathing were attached with different fastener spacing.

6) Monotonic capacity of fully sheathed steel-frame walls was comparable to that of wood-frame walls.

7) In monotonic and cyclic tests, steel-frame walls degraded in abrupt, stepwise manner due to bending of framing elements and pulling heads of sheathing screws through sheathing arbitrarily along the studs or top and bottom tracks. Sometimes, sheathing screws tore through panel edges. No fatigue of mechanical connections was observed.

REFERENCES

1. American Forest & Paper Association (AF&PA), 1995, *Wood Frame Construction Manual for One- and Two- Family Dwellings - SBC High Wind Edition*, American Forest & Paper Association, Washington, D.C.

2. American Society for Testing and Materials, 1995, *Proposed Standard Method for Dynamic Properties of Connections Assembled with Mechanical Fasteners* (*4th Draft*), ASTM, Philadelphia, PA.

3. American Iron and Steel Institute (AISI), 1996, *Builder's Steel Stud Guide*, Publication RG-9607, AISI, Washington, D.C.

4. Building Seismic Safety Council (BSSC), 1997, *NEHRP Recommended Provisions for Seismic Regulations for New Buildings and Other Structures*, BSSC, Washington, D.C.

5. Dolan, J.D. and A.C. Johnson, 1996, *Monotonic Tests of Long Shear Walls with Openings*, Virginia Polytechnic Institute and State University Timber Engineering Report TE-1996-001

6. Dolan, J.D. and A.C. Johnson, 1996, *Cyclic Tests of Long Shear Walls with Openings*. Virginia Polytechnic Institute and State University Timber Engineering Report TE-1996-002

7. Heine, C.P., 1997, *Effect of Overturning Restraint on the Performance of Fully Sheathed and Perforated Timber Framed Shear Walls*, Thesis submitted in partial fulfillment of Master's of Science Degree in Civil Engineering. Virginia Polytechnic Institute and State University, Blacksburg, VA

8. International Code Council, 1998, *International Building Code 2000*, Final Draft, ICC, Falls Church, VA

9. International Conference of Building Officials (ICBO), 1997, *Uniform Building Code*, ICBO, Whitter, CA

10. Johnson, A.C., 1997, *Monotonic and Cyclic Performance of Full-Scale Timber Shear Walls with Openings*, Thesis submitted in partial fulfillment of Master's of Science Degree in Civil Engineering. Virginia Polytechnic Institute and State University, Blacksburg, VA

11. Karacabeyli, E. and A. Ceccotti, 1998. Nailed Wood-Framed Shear Walls for Seismic Load: Test Results and Design Considerations. Proceedings of the Structural Engineers World Congress. San Francisco, CA T207-6.

12. Patton-Mallory, M., Gutkowski, R.M., and Soltis, L.A., 1984, *Racking Performance of Light-Frame Walls Sheathed on Two Sides,* Research paper FPL 448, USDA Forest Service, Forest Products Laboratory, Madison, WI

13. Porter, M.L., 1987, Sequential Phased Displacement (SPD) Procedure for TCCMAR Testing. *Proceedings of the Third Meeting of the Joint Technical Coordinating Committee on Masonry Research*, U.S. - Japan Coordinated Earthquake Research Program, Tomamu, Japan

14. Rose, J.D., 1998, *Preliminary Testing of Wood Structural Panel Shear Walls under Cyclic (Reversed) Loading,* APA Research Report 158, APA – The Engineered Wood Association, Tacoma, WA

15. Rose, J.D. and Keith, E.L., 1996, *Wood Structural Panel Shear Walls with Gypsum Wallboard and Window/Door Openings,* APA Research Report 157, APA – The Engineered Wood Association, Tacoma, WA

16. Serrette, R., G. Hall, and J. Ngyen, 1996, *Shear Wall Values for Light-Weight Steel Framing*. Research Report prepared for American Iron and Steel Institute, Washington, D.C. 56 pp.

17. Serrette, R., 1997, *Additional Shear Wall Values for Light Weight Steel Framing* Research Report No. LGSRG-1-97 Research Report prepared for American Iron and Steel Institute, Washington, D.C. 78 pp.

18. *Standard Building Code*, 1994 with 1996 Revisions, Southern Building Code Congress International, Birmingham, AL

19. Structural Engineers Association of Southern California (SEAOSC), 1997, *Standard Method of Cyclic (Reversed) Load Tests for Shear Resistance of Framed Walls for Buildings*, SEAOSC, Whitter, CA

20. Sugiyama, H. and T. Matsumoto, 1993, A Simplified Method of Calculating the Shear Strength of a Plywood-Sheathed Wall with Openings II. Analysis of the Shear Resistance and Deformation of a Shear Wall with Openings, *Mokuzai Gakkaishi*, 39(8): 924-929

21. Sugiyiama, H. and T. Matsumoto, 1994, Empirical Equations for the Estimation of Racking Strength of a Plywood-Sheathed Shear Wall with Openings. *Transactions of the Architectural Institute of Japan*

22. Yasumura, M. and H. Sugiyama, 1984, Shear properties of plywood-sheathed wall panels with opening. *Transactions of the Architectural Institute of Japan*, 338(4), 88-98

APPENDIX A

Table A. 1 - Specimen Amongyp1

Specimen	**Amongyp1**	For total length	
Ratio	**1.00**	**monotonic**	
Full-height length		**40 ft.**	**12.19 m**
		units	**Amongyp1**
Peak load, F_{peak}		Kips	40.337
		kN	179.419
Drift at peak load, Δ_{peak}		in.	1.163
		mm	29.54
Yield load, F_{yield}		Kips	35.450
		kN	157.680
Drift at yield load, Δ_{yield}		in.	0.374
		mm	9.49
Proportional limit, $0.4F_{max}$		Kips	16.135
		kN	71.768
Drift at prop. limit, $\Delta@0.4F_{max}$		in.	0.170
		mm	4.32
Failure load or $0.8F_{max}$		Kips	32.253
		kN	143.461
Drift at failure, $\Delta_{failure}$		in.	2.057
		mm	52.24
Elastic stiffness, E		Kip/in.	94.911
		kN/mm	16.621
Work until failure		Kip·ft.	5.524
		kN·m	7.489
Load @ .32 in.		Kips	23.633
Load @ .48 in.		Kips	29.326
Load @ .96 in.		Kips	38.967
Load @ 1.6 in.		Kips	35.906
$D = \Delta_{failure}/\Delta_{yield}$			5.506
$C_d^* = \Delta_{peak}/\Delta_{elastic}$			2.181
$R_d = \Delta_{peak}/\Delta_{yield}$			3.114
$R_d^* = \Delta_{design}/\Delta_{yield}$			3.114
$\Delta_{failure}/\Delta_{peak}$			1.768

Table A. 2 - Specimen Amon

Specimen	**Amon**	For total length	
Ratio	**1.00**	**monotonic**	
Full-height length		**40 ft.**	**12.19 m**
		units	**Amon**
Peak load, F_{peak}		Kips	32.549
		kN	144.778
Drift at peak load, Δ_{peak}		in.	1.488
		mm	37.80
Yield load, F_{yield}		Kips	28.092
		kN	124.954
Drift at yield load, Δ_{yield}		in.	0.411
		mm	10.43
Proportional limit, $0.4F_{max}$		Kips	13.020
		kN	57.911
Drift at prop. limit, $\Delta@0.4F_{max}$		in.	0.190
		mm	4.84
Failure load or $0.8F_{max}$		Kips	25.996
		kN	115.630
Drift at failure, $\Delta_{failure}$		in.	2.051
		mm	52.09
Elastic stiffness, E		Kip/in.	68.380
		kN/mm	11.975
Work until failure		Kip·ft.	4.320
		kN·m	5.857
Load @ .32 in.		Kips	17.563
Load @ .48 in.		Kips	21.592
Load @ .96 in.		Kips	28.574
Load @ 1.6 in.		Kips	31.797
$D = \Delta_{failure}/\Delta_{yield}$			4.992
$C_d^* = \Delta_{peak}/\Delta_{elastic}$			2.791
$R_d = \Delta_{peak}/\Delta_{yield}$			3.623
$R_d^* = \Delta_{design}/\Delta_{yield}$			3.623
$\Delta_{failure}/\Delta_{peak}$			1.378

Table A. 3 - Specimen Bmon

Specimen	**Bmon**	For total length	
Ratio	**0.76**	**monotonic**	
Full-height length		**28 ft.**	**8.534 m**
		units	**Bmon**
Peak load, F_{peak}		Kips	20.732
		kN	92.216
Drift at peak load, Δ_{peak}		in.	2.185
		mm	55.50
Yield load, F_{yield}		Kips	18.517
		kN	82.362
Drift at yield load, Δ_{yield}		in.	0.457
		mm	11.60
Proportional limit, $0.4F_{max}$		Kips	8.293
		kN	36.886
Drift at prop. limit, $\Delta@0.4F_{max}$		in.	0.205
		mm	5.20
Failure load or $0.8F_{max}$		Kips	16.570
		kN	73.703
Drift at failure, $\Delta_{failure}$		in.	2.548
		mm	64.73
Elastic stiffness, E		Kip/in.	40.532
		kN/mm	7.098
Work until failure		Kip·ft.	3.580
		kN·m	4.853
Load @ .32 in.		Kips	11.118
Load @ .48 in.		Kips	14.207
Load @ .96 in.		Kips	19.417
Load @ 1.6 in.		Kips	19.094
$D = \Delta_{failure}/\Delta_{yield}$			5.578
$C_d^* = \Delta_{peak}/\Delta_{elastic}$			4.097
$R_d = \Delta_{peak}/\Delta_{yield}$			4.783
$R_d^* = \Delta_{design}/\Delta_{yield}$			4.783
$\Delta_{failure}/\Delta_{peak}$			1.166

Table A. 4 - Specimen Cmon

Specimen	**Cmon**	For total length	
Ratio	**0.56**	**monotonic**	
Full-height length		**16 ft.**	**4.876 m**
		units	**Cmon**
Peak load, F_{peak}		Kips	13.857
		kN	61.636
Drift at peak load, Δ_{peak}		in.	2.089
		mm	53.06
Yield load, F_{yield}		Kips	12.576
		kN	55.938
Drift at yield load, Δ_{yield}		in.	0.538
		mm	13.68
Proportional limit, $0.4F_{max}$		Kips	5.543
		kN	24.654
Drift at prop. limit, $\Delta@0.4F_{max}$		in.	0.237
		mm	6.03
Failure load or $0.8F_{max}$		Kips	11.064
		kN	49.213
Drift at failure, $\Delta_{failure}$		in.	2.438
		mm	61.91
Elastic stiffness, E		Kip/in.	23.358
		kN/mm	4.090
Work until failure		Kip·ft.	2.272
		kN·m	3.081
Load @ .32 in.		Kips	6.902
Load @ .48 in.		Kips	8.889
Load @ .96 in.		Kips	12.085
Load @ 1.6 in.		Kips	13.347
$D = \Delta_{failure}/\Delta_{yield}$			4.527
$C_d^* = \Delta_{peak}/\Delta_{elastic}$			3.917
$R_d = \Delta_{peak}/\Delta_{yield}$			3.880
$R_d^* = \Delta_{design}/\Delta_{yield}$			3.880
$\Delta_{failure}/\Delta_{peak}$			1.167

Table A. 5 - Specimen Dmon

Specimen	**Dmon**	For total length	
Ratio	**0.48**	**monotonic**	
Full-height length		**16 ft.**	**4.876 m**
		units	**Dmon**
Peak load, F_{peak}		Kips	12.837
		kN	57.099
Drift at peak load, Δ_{peak}		in.	1.840
		mm	46.73
Yield load, F_{yield}		Kips	11.596
		kN	51.578
Drift at yield load, Δ_{yield}		in.	0.756
		mm	19.19
Proportional limit, $0.4F_{max}$		Kips	5.135
		kN	22.840
Drift at prop. limit, $\Delta@0.4F_{max}$		in.	0.335
		mm	8.50
Failure load or $0.8F_{max}$		Kips	10.259
		kN	45.632
Drift at failure, $\Delta_{failure}$		in.	2.514
		mm	63.85
Elastic stiffness, E		Kip/in.	15.345
		kN/mm	2.687
Work until failure		Kip·ft.	2.064
		kN·m	2.798
Load @ .32 in.		Kips	4.968
Load @ .48 in.		Kips	6.633
Load @ .96 in.		Kips	10.313
Load @ 1.6 in.		Kips	12.461
$D = \Delta_{failure}/\Delta_{yield}$			3.326
$C_d^* = \Delta_{peak}/\Delta_{elastic}$			3.450
$R_d = \Delta_{peak}/\Delta_{yield}$			2.435
$R_d^* = \Delta_{design}/\Delta_{yield}$			2.435
$\Delta_{failure}/\Delta_{peak}$			1.366

Table A. 6 - Specimen Emon

Specimen	**Emon**	For total length	
Ratio	**0.30**	**monotonic**	
Full-height length		**12 ft.**	**3.657 m**
		units	**Emon**
Peak load, F_{peak}		Kips	7.681
		kN	34.165
Drift at peak load, Δ_{peak}		in.	2.848
		mm	72.33
Yield load, F_{yield}		Kips	6.733
		kN	29.949
Drift at yield load, Δ_{yield}		in.	0.815
		mm	20.71
Proportional limit, $0.4F_{max}$		Kips	3.072
		kN	13.666
Drift at prop. limit, $\Delta@0.4F_{max}$		in.	0.372
		mm	9.45
Failure load or $0.8F_{max}$		Kips	6.042
		kN	26.875
Drift at failure, $\Delta_{failure}$		in.	4.310
		mm	109.46
Elastic stiffness, E		Kip/in.	8.257
		kN/mm	1.446
Work until failure		Kip·ft.	2.189
		kN·m	2.968
Load @ .32 in.		Kips	2.766
Load @ .48 in.		Kips	3.652
Load @ .96 in.		Kips	5.210
Load @ 1.6 in.		Kips	6.392
$D = \Delta_{failure}/\Delta_{yield}$			5.285
$C_d^* = \Delta_{peak}/\Delta_{elastic}$			5.339
$R_d = \Delta_{peak}/\Delta_{yield}$			3.492
$R_d^* = \Delta_{design}/\Delta_{yield}$			2.943
$\Delta_{failure}/\Delta_{peak}$			1.513

Table A. 7 - Specimen Acyc1

Specimen	**Acyc1**	For total length		
Ratio	**1.00**	**cyclic**		
Full-height length		**40 ft.**	**12.19 m**	
		units	**initial**	**stabilized**
Peak load, F_{peak}		Kips	25.794	20.799
		kN	114.734	92.516
Drift at peak load, Δ_{peak}		in.	1.310	1.207
		mm	33.26	30.66
Yield load, F_{yield}		Kips	23.280	18.885
		kN	103.550	84.001
Drift at yield load, Δ_{yield}		in.	0.398	0.314
		mm	10.12	7.97
Proportional limit, $0.4F_{max}$		Kips	10.318	8.320
		kN	45.894	37.006
Drift at prop. limit, $\Delta@0.4F_{max}$		in.	0.177	0.138
		mm	4.49	3.51
Failure load or $0.8F_{max}$		Kips	20.636	16.640
		kN	91.787	74.013
Drift at failure, $\Delta_{failure}$		in.	1.677	1.563
		mm	42.59	39.70
Elastic stiffness, E $@0.4F_{max}$		Kip/in.	58.472	60.158
		kN/mm	10.239	10.535
Work until failure		Kip·ft.	31.122	30.272
		kN·m	42.194	41.041
Load @ .32 in.		Kips	15.545	14.055
Load @ .48 in.		Kips	19.205	16.782
Load @ .96 in.		Kips	24.910	20.468
Load @ 1.6 in.		Kips	22.187	15.658
$D = \Delta_{failure}/\Delta_{yield}$			4.209	4.984
$C_d^* = \Delta_{peak}/\Delta_{elastic}$			2.455	2.263
$R_d = \Delta_{peak}/\Delta_{yield}$			1.507	1.950
$R_d^* = \Delta_{design}/\Delta_{yield}$			3.290	3.848
$\Delta_{failure}/\Delta_{peak}$			1.291	1.295
$\zeta_{eq} = W_D/U_0/4\pi$			0.081	0.059

Note: ζ_{eq} at F_{max}

Table A. 8 - Specimen Acyc2

Specimen	**Acyc2**	For total length		
Ratio	**1.00**	**cyclic**		
Full-height length		**40 ft.**	**12.19 m**	
		units	**initial**	**stabilized**
Peak load, F_{peak}		Kips	27.661	22.559
		kN	123.036	100.340
Drift at peak load, Δ_{peak}		in.	1.311	1.103
		mm	33.30	28.02
Yield load, F_{yield}		Kips	25.019	20.380
		kN	111.284	90.652
Drift at yield load, Δ_{yield}		in.	0.359	0.278
		mm	9.12	7.06
Proportional limit, $0.4F_{max}$		Kips	11.064	9.023
		kN	49.214	40.136
Drift at prop. limit, $\Delta@0.4F_{max}$		in.	0.159	0.123
		mm	4.03	3.12
Failure load or $0.8F_{max}$		Kips	22.129	18.047
		kN	98.429	80.272
Drift at failure, $\Delta_{failure}$		in.	1.688	1.597
		mm	42.89	40.56
Elastic stiffness, E $@0.4F_{max}$		Kip/in.	69.706	73.308
		kN/mm	12.207	12.838
Work until failure		Kip·ft.	32.782	31.799
		kN·m	44.444	43.112
Load @ .32 in.		Kips	17.946	16.009
Load @ .48 in.		Kips	21.641	18.745
Load @ .96 in.		Kips	26.916	22.202
Load @ 1.6 in.		Kips	23.357	17.928
$D = \Delta_{failure}/\Delta_{yield}$			4.703	5.761
$C_d^* = \Delta_{peak}/\Delta_{elastic}$			2.458	2.068
$R_d = \Delta_{peak}/\Delta_{yield}$			1.679	1.882
$R_d^* = \Delta_{design}/\Delta_{yield}$			3.653	3.964
$\Delta_{failure}/\Delta_{peak}$			1.299	1.461
$\zeta_{eq} = W_D/U_0/4\pi$			0.078	0.058

Note: ζ_{eq} at F_{max}

Table A. 9- Specimen Bcyc1

Specimen	**Bcyc1**	For total length		
Ratio	**0.76**	**cyclic**		
Full-height length		**28 ft.**	**8.534 m**	
		units	**initial**	**stabilized**
Peak load, F_{peak}		Kips	19.792	16.799
		kN	88.037	74.720
Drift at peak load, Δ_{peak}		in.	1.412	1.201
		mm	35.87	30.51
Yield load, F_{yield}		Kips	17.608	14.991
		kN	78.319	66.679
Drift at yield load, Δ_{yield}		in.	0.523	0.454
		mm	13.28	11.54
Proportional limit, $0.4F_{max}$		Kips	7.917	6.719
		kN	35.215	29.888
Drift at prop. limit, $\Delta@0.4F_{max}$		in.	0.235	0.204
		mm	5.97	5.17
Failure load or $0.8F_{max}$		Kips	15.834	13.439
		kN	70.430	59.776
Drift at failure, $\Delta_{failure}$		in.	1.867	1.737
		mm	47.43	44.12
Elastic stiffness, E $@0.4F_{max}$		Kip/in.	33.681	33.086
		kN/mm	5.898	5.794
Work until failure		Kip·ft.	28.913	28.100
		kN·m	39.199	38.097
Load @ .32 in.		Kips	9.912	9.246
Load @ .48 in.		Kips	12.716	11.601
Load @ .96 in.		Kips	18.324	15.989
Load @ 1.6 in.		Kips	18.246	15.680
$D = \Delta_{failure}/\Delta_{yield}$			3.571	3.831
$C_d^* = \Delta_{peak}/\Delta_{elastic}$			2.648	2.252
$R_d = \Delta_{peak}/\Delta_{yield}$			1.364	1.384
$R_d^* = \Delta_{design}/\Delta_{yield}$			2.700	2.649
$\Delta_{failure}/\Delta_{peak}$			1.322	1.446
$\zeta_{eq} = W_D/U_0/4\pi$			0.077	0.060

Note: ζ_{eq} at F_{max}

Table A. 10 - Specimen Bcyc2

Specimen	**Bcyc2**	For total length		
Ratio	**0.76**	**cyclic**		
Full-height length		**28 ft.**	**8.534 m**	
		units	**initial**	**stabilized**
Peak load, F_{peak}		Kips	21.283	18.194
		kN	94.667	80.929
Drift at peak load, Δ_{peak}		in.	1.406	1.403
		mm	35.72	35.65
Yield load, F_{yield}		Kips	18.725	16.033
		kN	83.287	71.313
Drift at yield load, Δ_{yield}		in.	0.556	0.483
		mm	14.11	12.28
Proportional limit, $0.4F_{max}$		Kips	8.513	7.278
		kN	37.867	32.372
Drift at prop. limit, $\Delta@0.4F_{max}$		in.	0.253	0.219
		mm	6.42	5.57
Failure load or $0.8F_{max}$		Kips	17.026	14.556
		kN	75.733	64.743
Drift at failure, $\Delta_{failure}$		in.	1.933	1.769
		mm	49.11	44.93
Elastic stiffness, E $@0.4F_{max}$		Kip/in.	33.687	33.166
		kN/mm	5.899	5.808
Work until failure		Kip·ft.	32.179	31.012
		kN·m	43.626	42.045
Load @ .32 in.		Kips	10.040	9.366
Load @ .48 in.		Kips	12.807	11.680
Load @ .96 in.		Kips	18.801	16.573
Load @ 1.6 in.		Kips	20.371	17.816
$D = \Delta_{failure}/\Delta_{yield}$			3.482	3.659
$C_d^* = \Delta_{peak}/\Delta_{elastic}$			2.637	2.631
$R_d = \Delta_{peak}/\Delta_{yield}$			1.231	1.460
$R_d^* = \Delta_{design}/\Delta_{yield}$			2.533	2.903
$\Delta_{failure}/\Delta_{peak}$			1.375	1.260
$\zeta_{eq} = W_D/U_0/4\pi$			0.075	0.059

Note: ζ_{eq} at F_{max}

Table A. 2 - Specimen Ccyc1

Specimen	**Ccyc**	For total length		
Ratio	**0.56**	**cyclic**		
Full-height length		**16 ft.**	**4.876 m**	
		units	**initial**	**stabilized**
Peak load, F_{peak}		Kips	13.509	11.628
		kN	60.086	51.724
Drift at peak load, Δ_{peak}		in.	1.310	1.405
		mm	33.26	35.68
Yield load, F_{yield}		Kips	12.089	10.448
		kN	53.773	46.474
Drift at yield load, Δ_{yield}		in.	0.491	0.443
		mm	12.47	11.25
Proportional limit, $0.4F_{max}$		Kips	5.403	4.651
		kN	24.034	20.689
Drift at prop. limit, $\Delta@0.4F_{max}$		in.	0.219	0.197
		mm	5.57	5.01
Failure load or $0.8F_{max}$		Kips	10.807	9.303
		kN	48.069	41.379
Drift at failure, $\Delta_{failure}$		in.	2.159	2.033
		mm	54.84	51.64
Elastic stiffness, E $@0.4F_{max}$		Kip/in.	24.639	23.595
		kN/mm	4.315	4.132
Work until failure		Kip·ft.	28.441	27.575
		kN·m	38.560	37.384
Load @ .32 in.		Kips	7.155	6.585
Load @ .48 in.		Kips	9.015	8.255
Load @ .96 in.		Kips	12.547	11.062
Load @ 1.6 in.		Kips	12.854	11.288
$D = \Delta_{failure}/\Delta_{yield}$			4.438	4.635
$C_d^* = \Delta_{peak}/\Delta_{elastic}$			2.455	2.634
$R_d = \Delta_{peak}/\Delta_{yield}$			1.347	1.484
$R_d^* = \Delta_{design}/\Delta_{yield}$			2.666	3.188
$\Delta_{failure}/\Delta_{peak}$			1.667	1.447
$\zeta_{eq} = W_D/U_0/4\pi$			0.076	0.059

Note: ζ_{eq} at F_{max}

Table A. 12 - Specimen Ccyc2

Specimen	**Ccyc2**	For total length		
Ratio	**0.56**	**cyclic**		
Full-height length		**16 ft.**	**4.876 m**	
		units	**initial**	**stabilized**
Peak load, F_{peak}		Kips	13.119	11.763
		kN	58.353	52.320
Drift at peak load, Δ_{peak}		in.	1.680	1.506
		mm	42.68	38.25
Yield load, F_{yield}		Kips	11.425	10.062
		kN	50.819	44.757
Drift at yield load, Δ_{yield}		in.	0.597	0.542
		mm	15.17	13.76
Proportional limit, $0.4F_{max}$		Kips	5.248	4.705
		kN	23.341	20.928
Drift at prop. limit, $\Delta@0.4F_{max}$		in.	0.274	0.253
		mm	6.97	6.43
Failure load or $0.8F_{max}$		Kips	10.495	9.410
		kN	46.683	41.856
Drift at failure, $\Delta_{failure}$		in.	2.703	2.372
		mm	68.65	60.25
Elastic stiffness, E $@0.4F_{max}$		Kip/in.	19.150	18.582
		kN/mm	3.354	3.254
Work until failure		Kip·ft.	33.585	28.821
		kN·m	45.533	39.075
Load @ .32 in.		Kips	5.816	5.515
Load @ .48 in.		Kips	7.414	6.885
Load @ .96 in.		Kips	11.545	10.331
Load @ 1.6 in.		Kips	12.962	11.531
$D = \Delta_{failure}/\Delta_{yield}$			4.526	4.378
$C_d^* = \Delta_{peak}/\Delta_{elastic}$			3.150	2.823
$R_d = \Delta_{peak}/\Delta_{yield}$			1.265	1.281
$R_d^* = \Delta_{design}/\Delta_{yield}$			2.821	2.783
$\Delta_{failure}/\Delta_{peak}$			1.621	1.584
$\zeta_{eq} = W_D/U_0/4\pi$			0.065	0.053

Note: ζ_{eq} at F_{max}

Table A. 13 - Specimen Dcyc1

Specimen	**Dcyc1**	For total length		
Ratio	**0.56**	**cyclic**		
Full-height length		**16 ft.**	**4.876 m**	
		units	**initial**	**stabilized**
Peak load, F_{peak}		Kips	11.132	9.775
		kN	49.513	43.481
Drift at peak load, Δ_{peak}		in.	1.607	1.614
		mm	40.82	41.00
Yield load, F_{yield}		Kips	10.172	8.822
		kN	45.247	39.239
Drift at yield load, Δ_{yield}		in.	0.617	0.557
		mm	15.68	14.15
Proportional limit, $0.4F_{max}$		Kips	4.453	3.910
		kN	19.805	17.393
Drift at prop. limit, $\Delta@0.4F_{max}$		in.	0.270	0.247
		mm	6.87	6.28
Failure load or $0.8F_{max}$		Kips	8.905	7.820
		kN	39.610	34.785
Drift at failure, $\Delta_{failure}$		in.	2.455	2.675
		mm	62.36	67.96
Elastic stiffness, E $@0.4F_{max}$		Kip/in.	16.497	15.877
		kN/mm	2.889	2.780
Work until failure		Kip·ft.	17.876	28.145
		kN·m	24.235	38.158
Load @ .32 in.		Kips	5.055	4.771
Load @ .48 in.		Kips	6.710	6.238
Load @ .96 in.		Kips	10.112	9.082
Load @ 1.6 in.		Kips	10.783	9.647
$D = \Delta_{failure}/\Delta_{yield}$			3.997	4.831
$C_d^* = \Delta_{peak}/\Delta_{elastic}$			3.013	3.027
$R_d = \Delta_{peak}/\Delta_{yield}$			1.499	1.692
$R_d^* = \Delta_{design}/\Delta_{yield}$			2.612	2.913
$\Delta_{failure}/\Delta_{peak}$			1.516	1.653
$\zeta_{eq} = W_D/U_0/4\pi$			0.074	0.062

Note: ζ_{eq} at F_{max}

Table A. 14 - Specimen Dcyc2

Specimen	**Dcyc2**	For total length		
Ratio	**0.56**	**cyclic**		
Full-height length		**16 ft.**	**4.876 m**	
		units	**initial**	**stabilized**
Peak load, F_{peak}		Kips	12.072	10.500
		kN	53.694	46.706
Drift at peak load, Δ_{peak}		in.	1.408	1.304
		mm	35.76	33.12
Yield load, F_{yield}		Kips	10.512	9.169
		kN	46.756	40.786
Drift at yield load, Δ_{yield}		in.	0.512	0.456
		mm	13.00	11.58
Proportional limit, $0.4F_{max}$		Kips	4.829	4.200
		kN	21.478	18.682
Drift at prop. limit, $\Delta@0.4F_{max}$		in.	0.235	0.209
		mm	5.97	5.31
Failure load or $0.8F_{max}$		Kips	9.657	8.400
		kN	42.955	37.365
Drift at failure, $\Delta_{failure}$		in.	2.291	2.102
		mm	58.18	53.40
Elastic stiffness, E $@0.4F_{max}$		Kip/in.	20.539	20.124
		kN/mm	3.597	3.524
Work until failure		Kip·ft.	21.604	20.740
		kN·m	29.289	28.119
Load @ .32 in.		Kips	5.995	5.584
Load @ .48 in.		Kips	7.445	6.780
Load @ .96 in.		Kips	10.699	9.626
Load @ 1.6 in.		Kips	11.449	9.831
$D = \Delta_{failure}/\Delta_{yield}$			4.473	4.620
$C_d^* = \Delta_{peak}/\Delta_{elastic}$			2.639	2.445
$R_d = \Delta_{peak}/\Delta_{yield}$			1.363	1.589
$R_d^* = \Delta_{design}/\Delta_{yield}$			2.751	2.868
$\Delta_{failure}/\Delta_{peak}$			1.627	1.617
$\zeta_{eq} = W_D/U_0/4\pi$			0.072	0.056

Note: ζ_{eq} at F_{max}

Table A. 15 - Specimen Ecyc1

Specimen	**Ecyc1**	For total length		
Ratio	**0.30**	**cyclic**		
Full-height length		**12 ft.**	**3.657 m**	
		units	**initial**	**stabilized**
Peak load, F_{peak}		Kips	6.445	5.653
		kN	28.670	25.145
Drift at peak load, Δ_{peak}		in.	1.910	1.598
		mm	48.52	40.59
Yield load, F_{yield}		Kips	5.656	4.931
		kN	25.159	21.933
Drift at yield load, Δ_{yield}		in.	0.611	0.542
		mm	15.53	13.78
Proportional limit, $0.4F_{max}$		Kips	2.578	2.261
		kN	11.468	10.058
Drift at prop. limit, $\Delta@0.4F_{max}$		in.	0.278	0.248
		mm	7.06	6.31
Failure load or $0.8F_{max}$		Kips	5.156	4.522
		kN	22.936	20.116
Drift at failure, $\Delta_{failure}$		in.	2.303	2.132
		mm	58.49	54.14
Elastic stiffness, E $@0.4F_{max}$		Kip/in.	9.280	9.111
		kN/mm	1.625	1.596
Work until failure		Kip·ft.	11.803	11.497
		kN·m	16.002	15.587
Load @ .32 in.		Kips	2.848	2.692
Load @ .48 in.		Kips	3.665	3.366
Load @ .96 in.		Kips	5.334	4.703
Load @ 1.6 in.		Kips	6.140	5.642
$D = \Delta_{failure}/\Delta_{yield}$			3.770	3.932
$C_d^* = \Delta_{peak}/\Delta_{elastic}$			3.582	2.997
$R_d = \Delta_{peak}/\Delta_{yield}$			1.524	1.504
$R_d^* = \Delta_{design}/\Delta_{yield}$			3.123	2.948
$\Delta_{failure}/\Delta_{peak}$			1.209	1.334
$\zeta_{eq} = W_D/U_0/4\pi$			0.066	0.052

Note: ζ_{eq} at F_{max}

Table A. 16 - Specimen Ecyc2

Specimen	**Ecyc2**	For total length		
Ratio	**0.30**	**cyclic**		
Full-height length		**12 ft.**	**3.657 m**	
		units	**initial**	**stabilized**
Peak load, F_{peak}		Kips	6.499	5.559
		kN	28.908	24.726
Drift at peak load, Δ_{peak}		in.	1.408	1.405
		mm	35.76	35.68
Yield load, F_{yield}		Kips	5.665	4.885
		kN	25.199	21.730
Drift at yield load, Δ_{yield}		in.	0.550	0.487
		mm	13.96	12.38
Proportional limit, $0.4F_{max}$		Kips	2.600	2.224
		kN	11.563	9.891
Drift at prop. limit, $\Delta@0.4F_{max}$		in.	0.252	0.222
		mm	6.41	5.63
Failure load or $0.8F_{max}$		Kips	5.199	4.447
		kN	23.126	19.781
Drift at failure, $\Delta_{failure}$		in.	1.835	1.719
		mm	46.61	43.67
Elastic stiffness, E $@0.4F_{max}$		Kip/in.	10.320	10.022
		kN/mm	1.807	1.755
Work until failure		Kip·ft.	8.473	8.174
		kN·m	11.487	11.082
Load @ .32 in.		Kips	3.105	2.936
Load @ .48 in.		Kips	4.012	3.741
Load @ .96 in.		Kips	5.697	5.062
Load @ 1.6 in.		Kips	6.133	4.905
$D = \Delta_{failure}/\Delta_{yield}$			3.371	3.539
$C_d^* = \Delta_{peak}/\Delta_{elastic}$			2.640	2.634
$R_d = \Delta_{peak}/\Delta_{yield}$			1.190	1.391
$R_d^* = \Delta_{design}/\Delta_{yield}$			2.576	2.887
$\Delta_{failure}/\Delta_{peak}$			1.304	1.224
$\zeta_{eq} = W_D/U_0/4\pi$			0.071	0.052

Note: ζ_{eq} at F_{max}

APPENDIX B

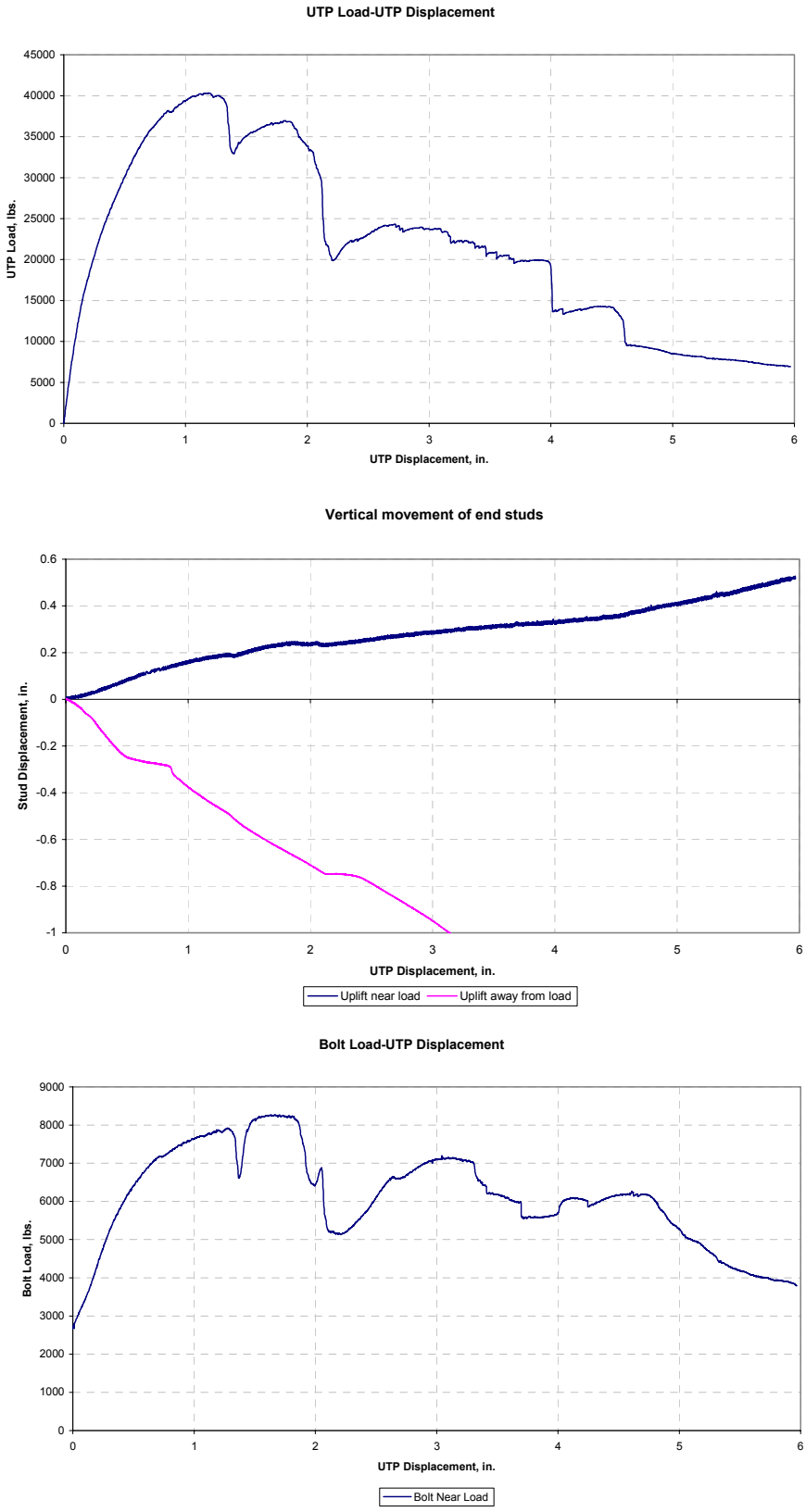

Figure B. 1- Specimen Amongyp1.

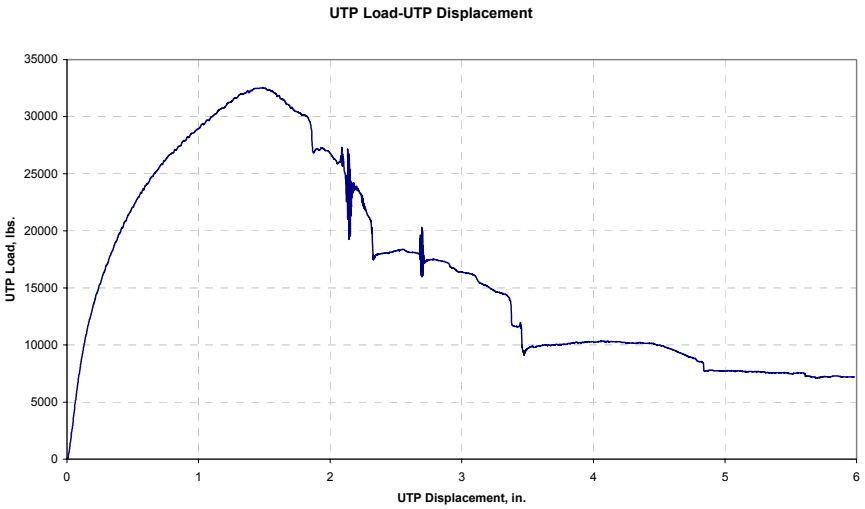

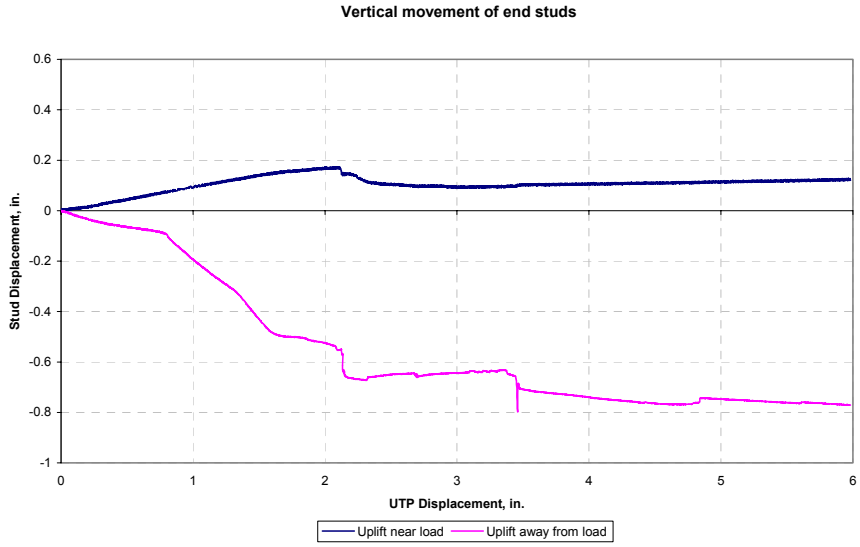

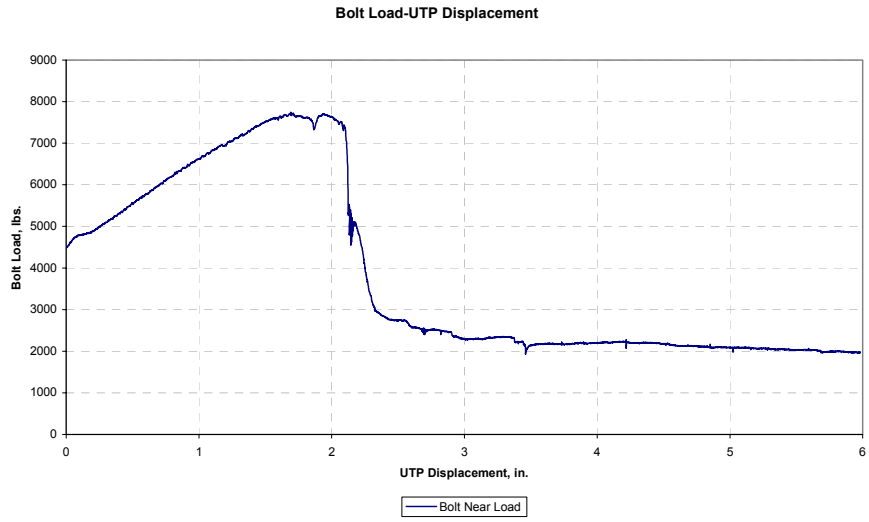

Figure B. 2 - Specimen Amon.

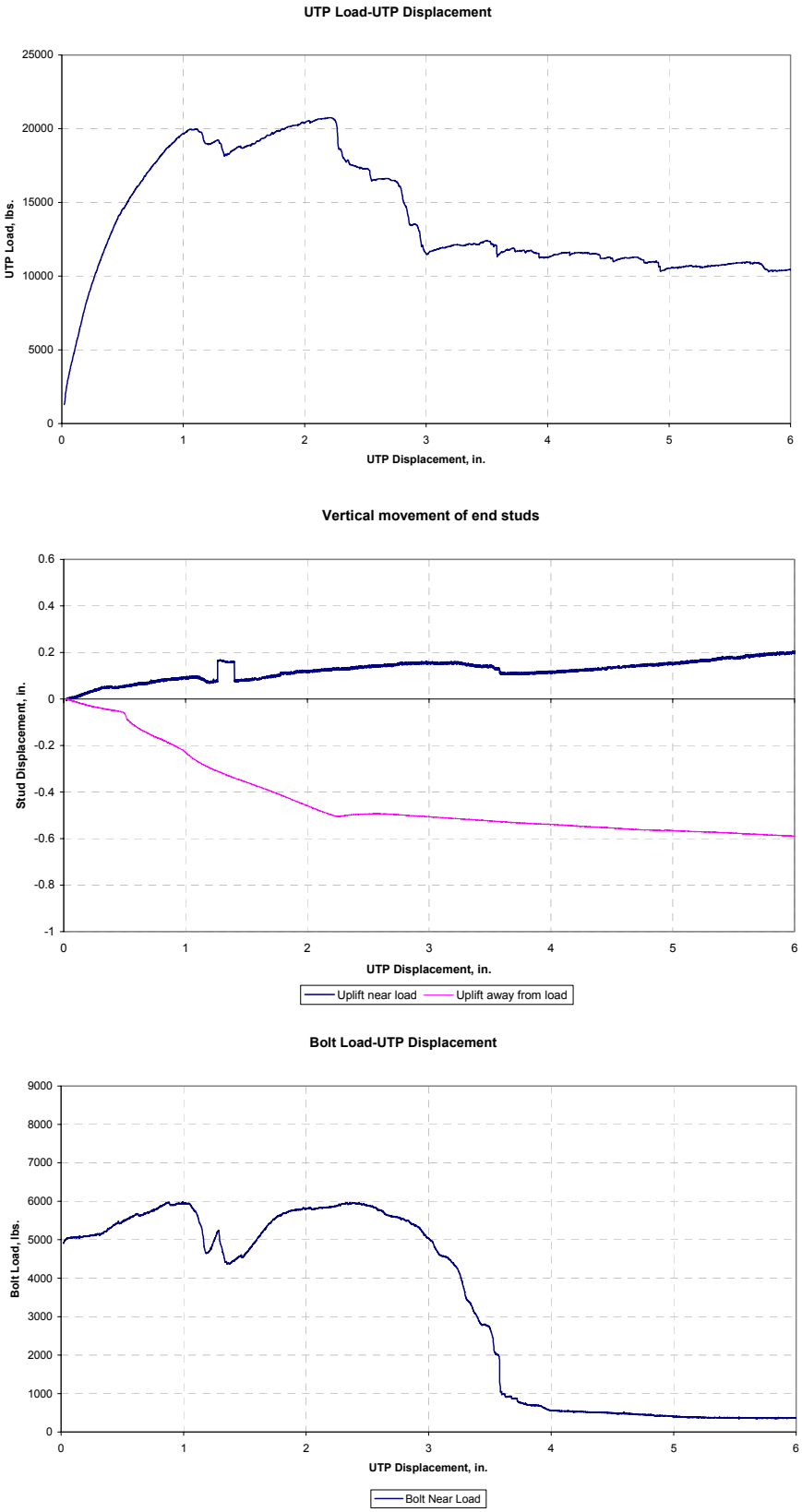

Figure B. 3 - Specimen Bmon.

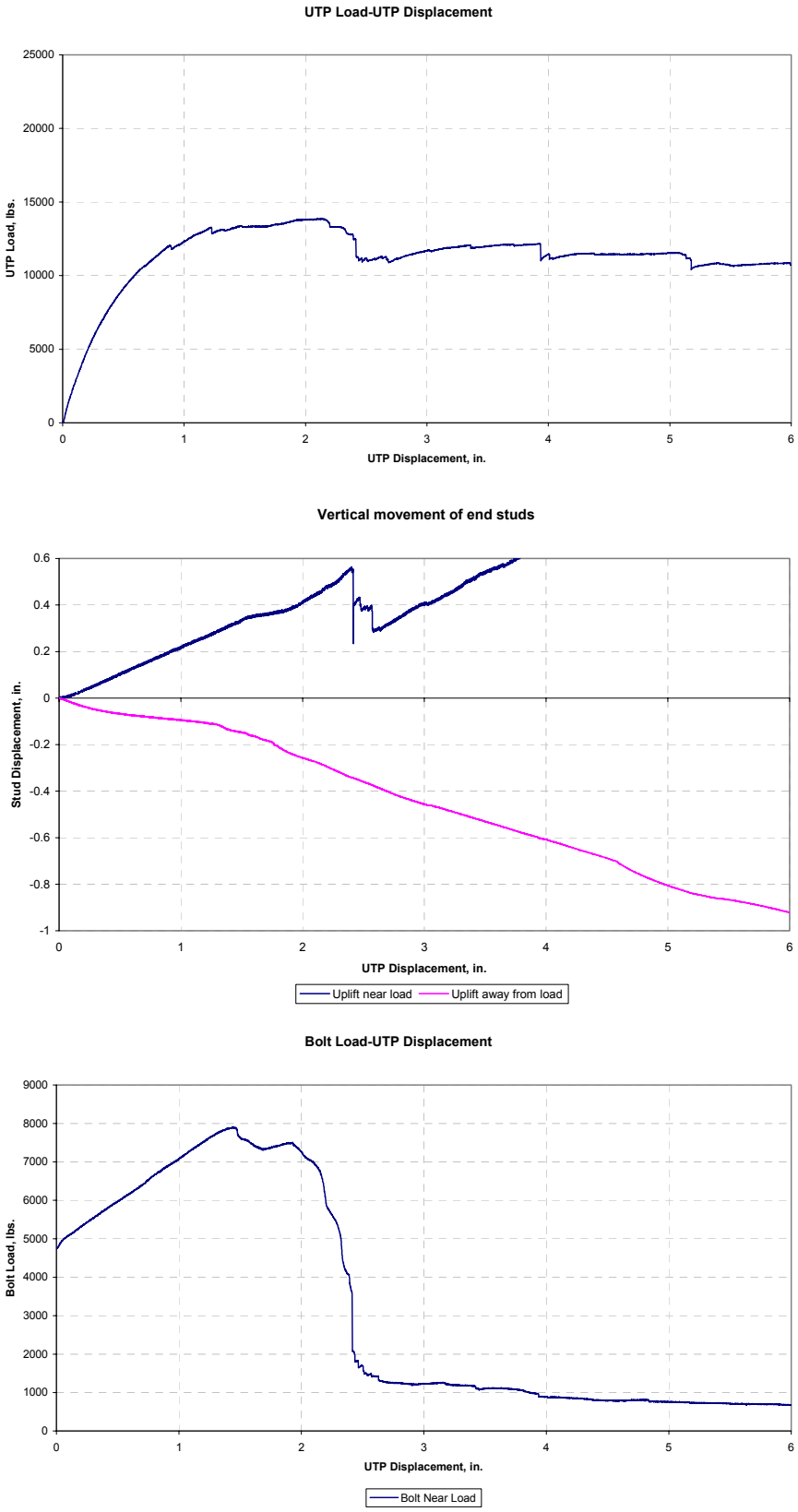

Figure B. 4 - Specimen Cmon.

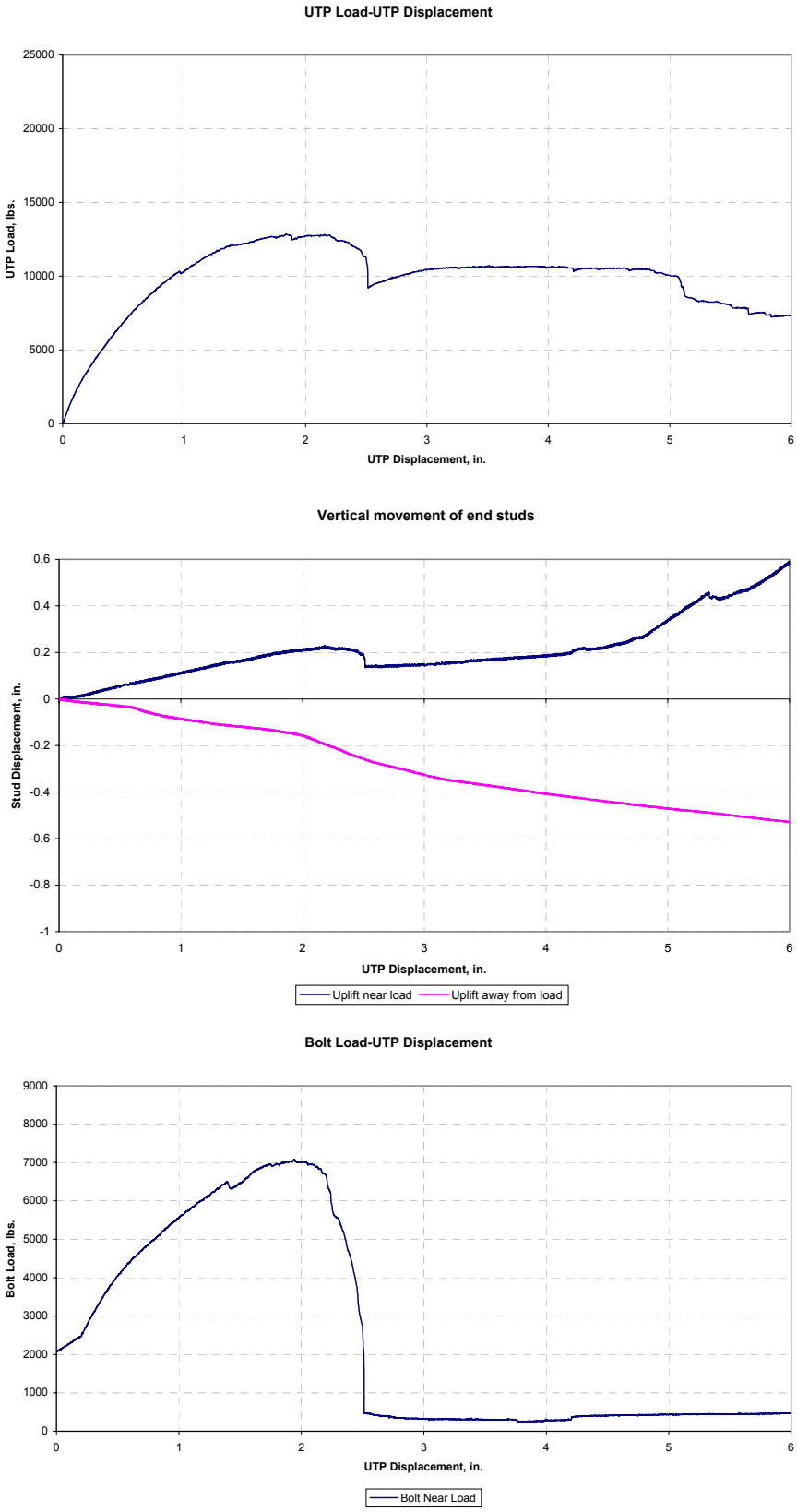

Figure B. 5 - Specimen Dmon.

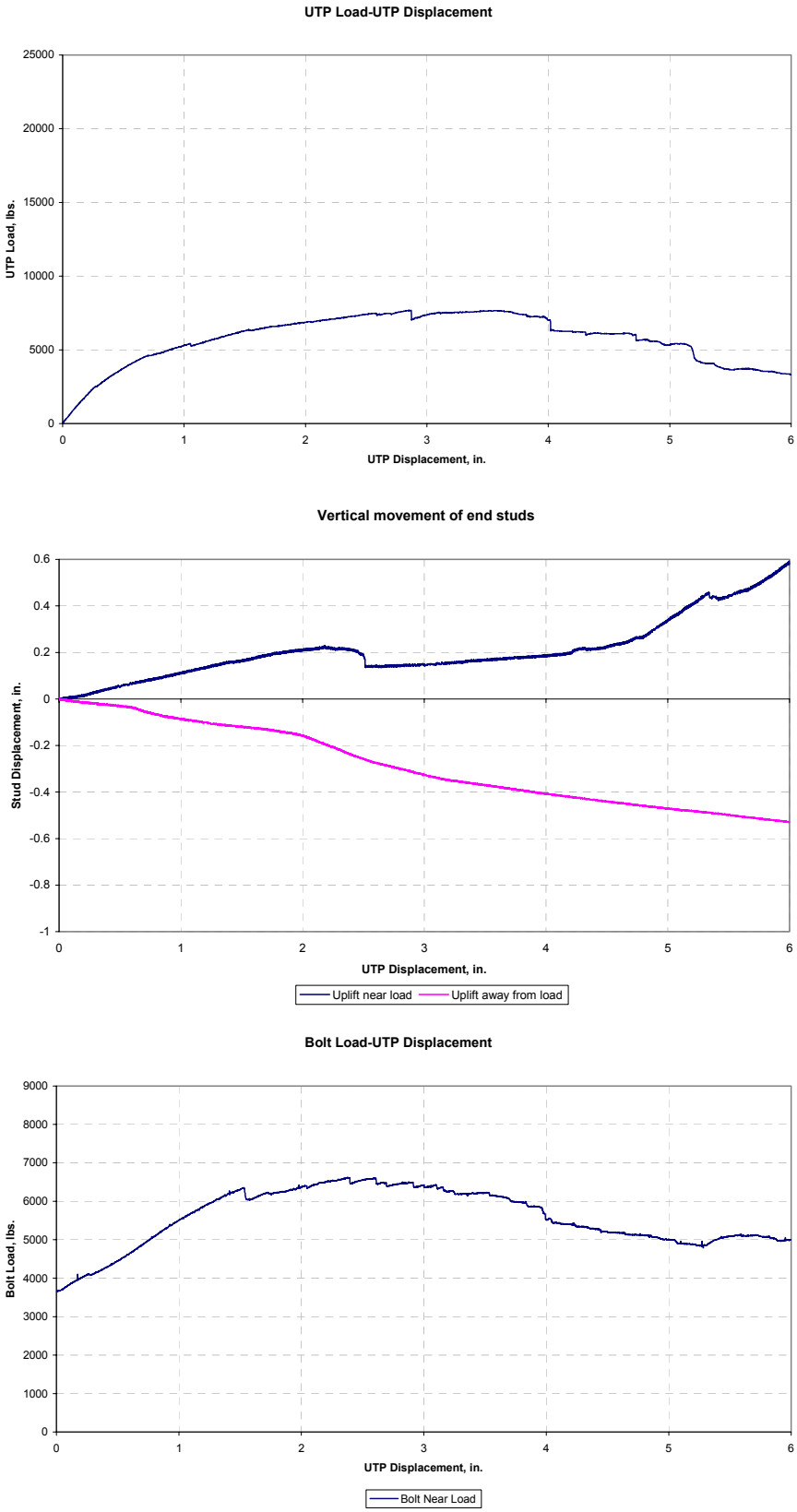

Figure B. 6 - Specimen Emon.

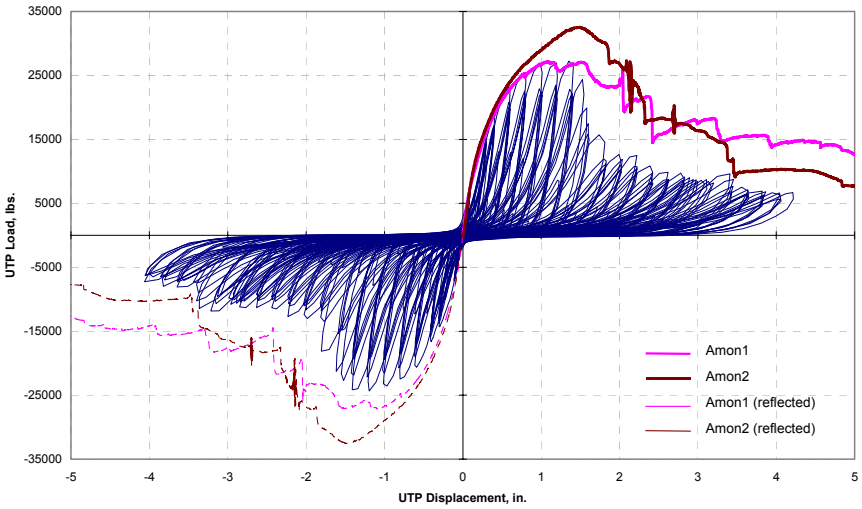

Vertical movement of end studs

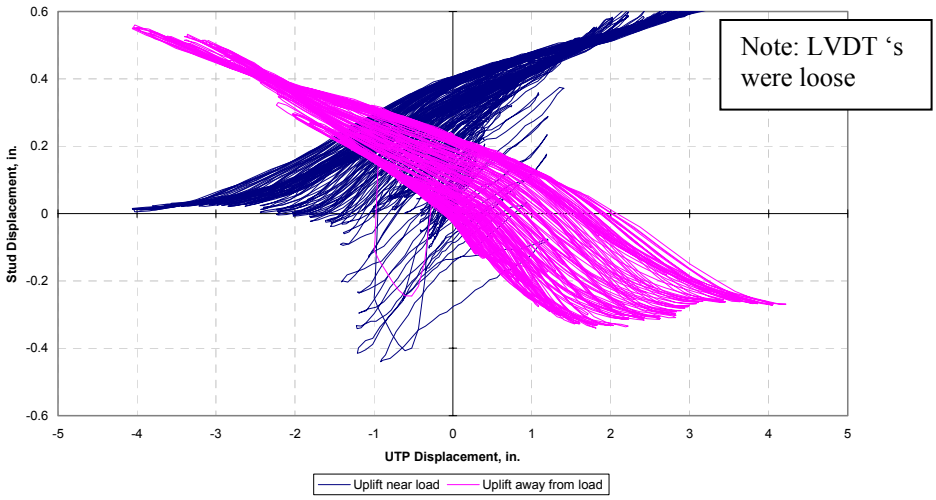

Bolt Load-UTP Displacement

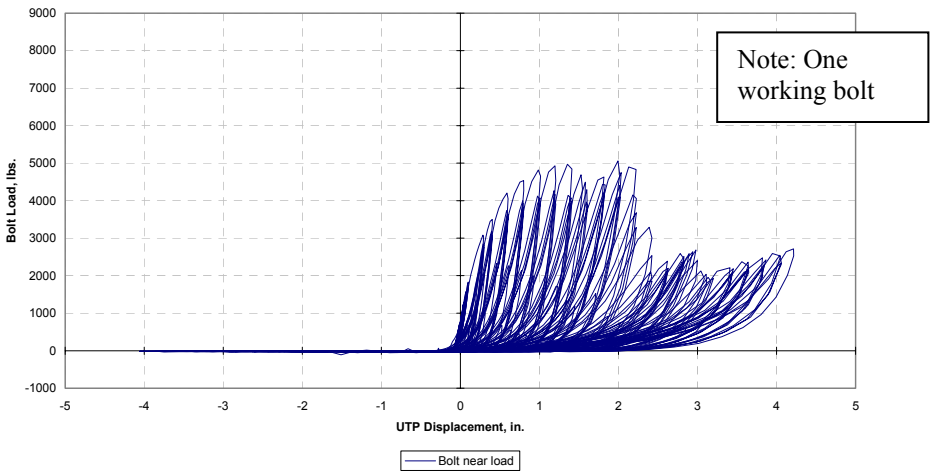

Figure B. 7 - Specimen Acyc1.

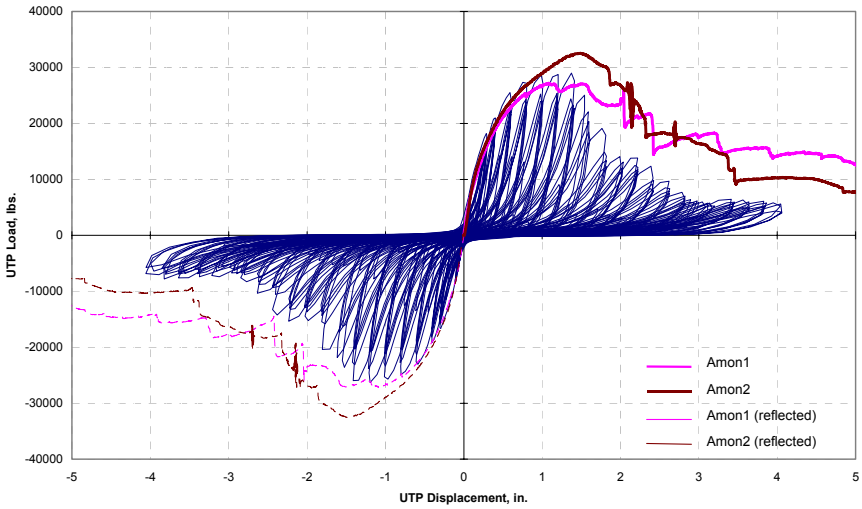

Vertical movement of end studs

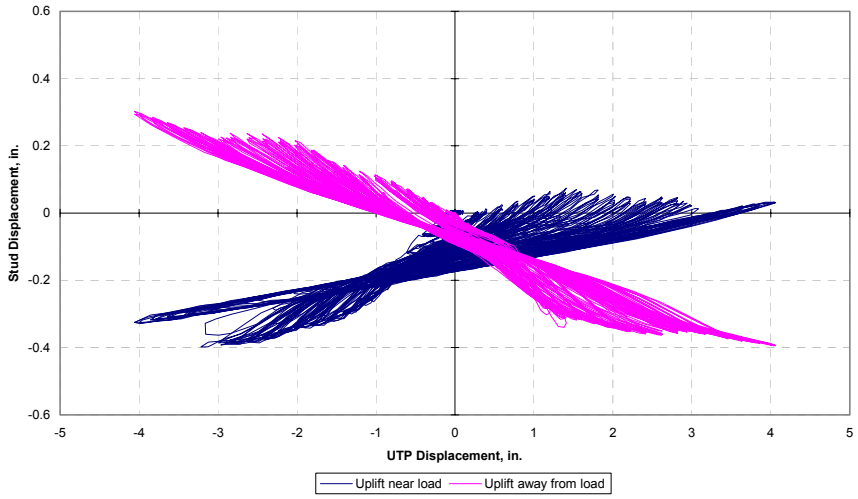

Bolt Load-UTP Displacement

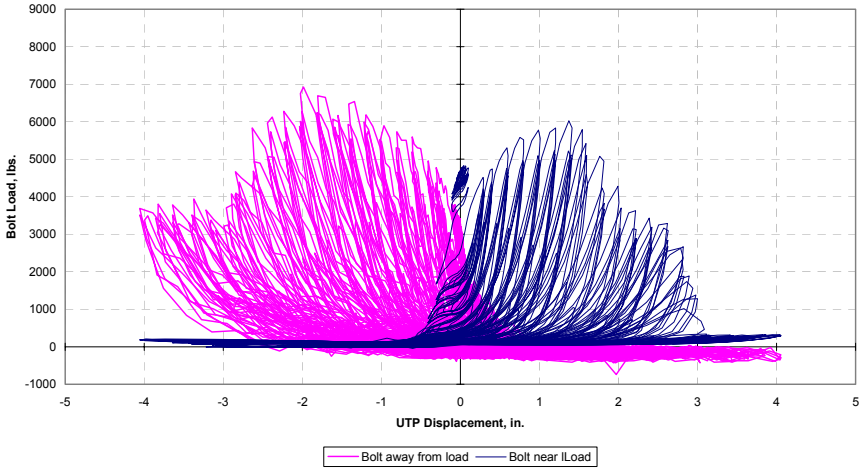

Figure B. 8 - Specimen Acyc2.

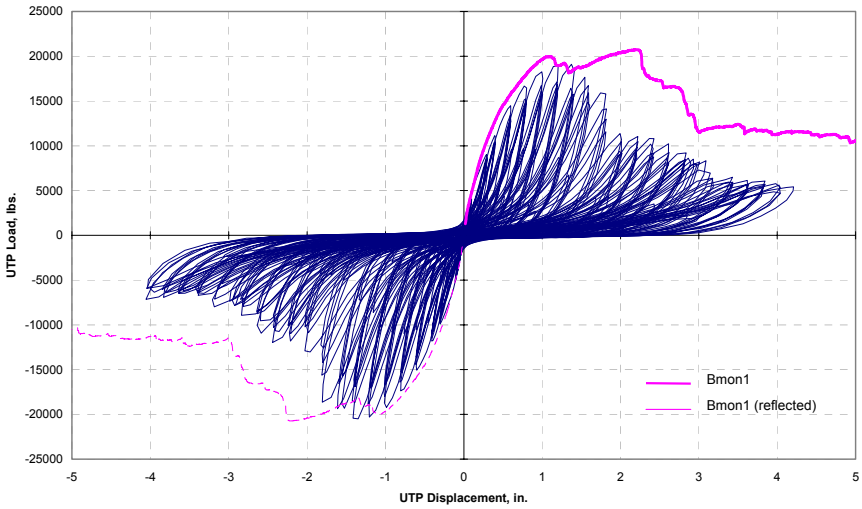

Vertical movement of end studs

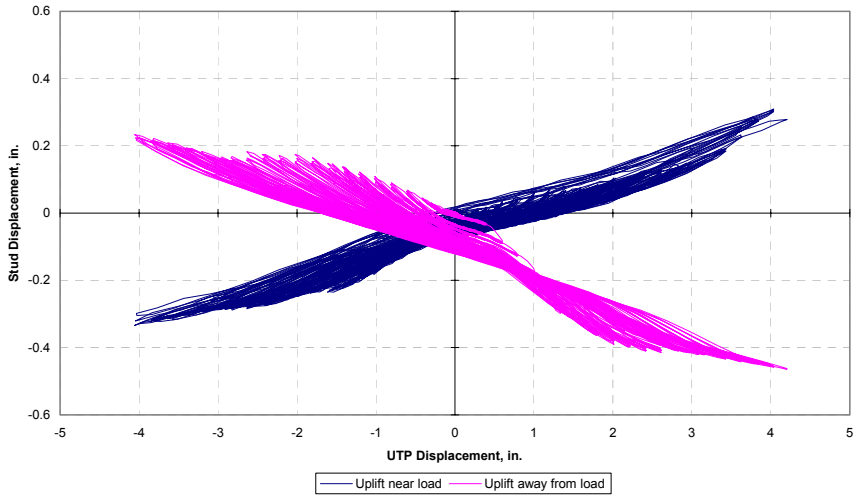

Bolt Load-UTP Displacement

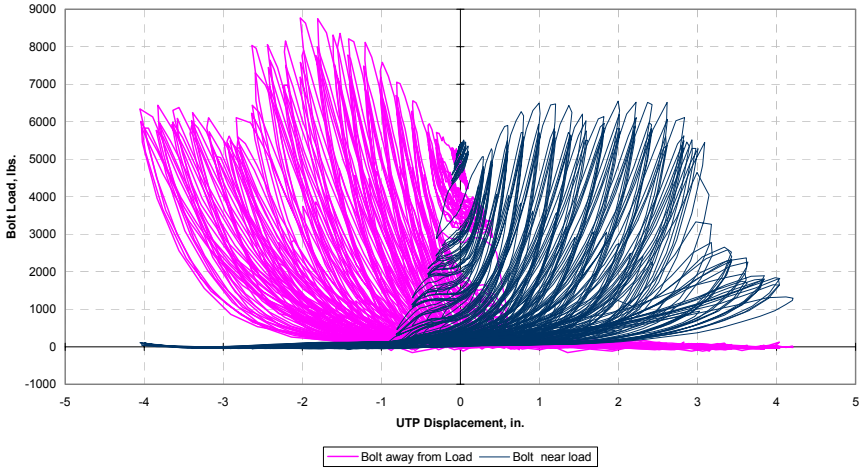

Figure B. 9 - Specimen Bcyc1.

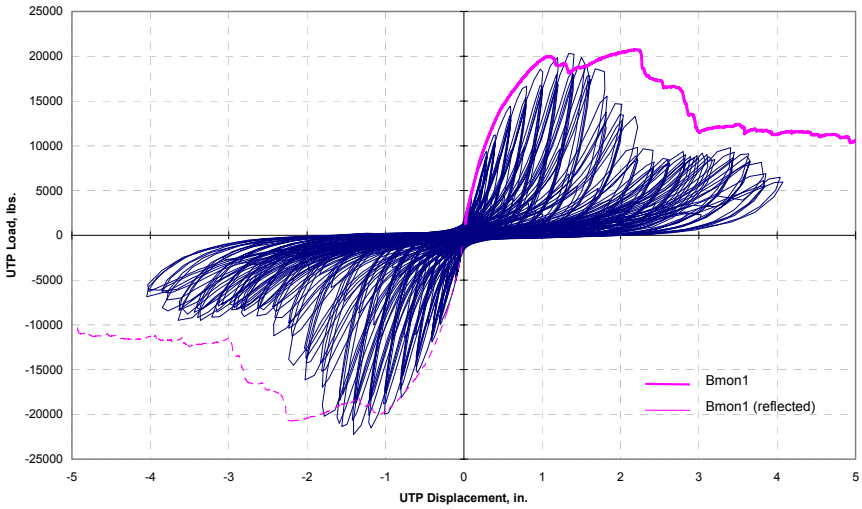

Vertical movement of end studs

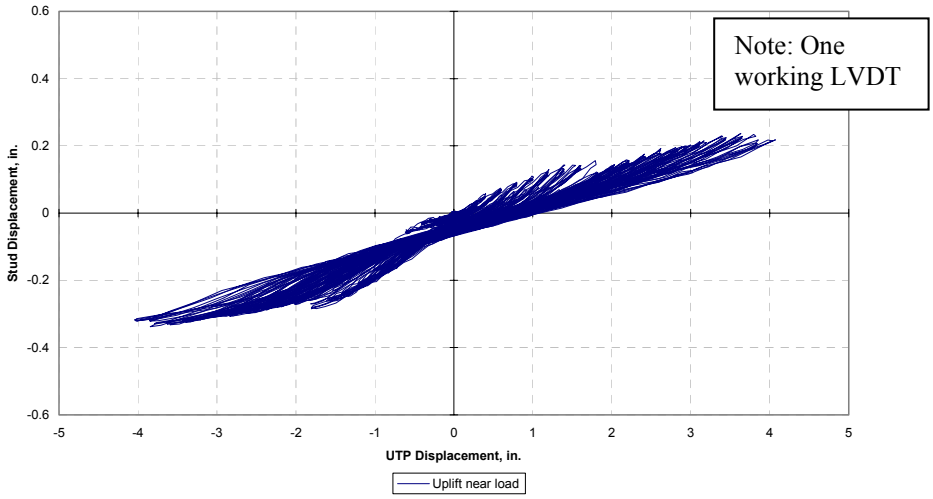

Bolt Load-UTP Displacement

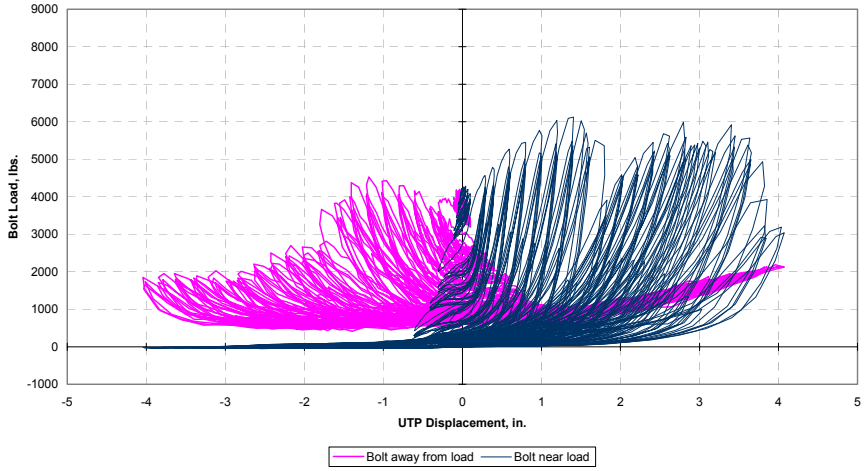

Figure B. 10 - Specimen Bcyc2.

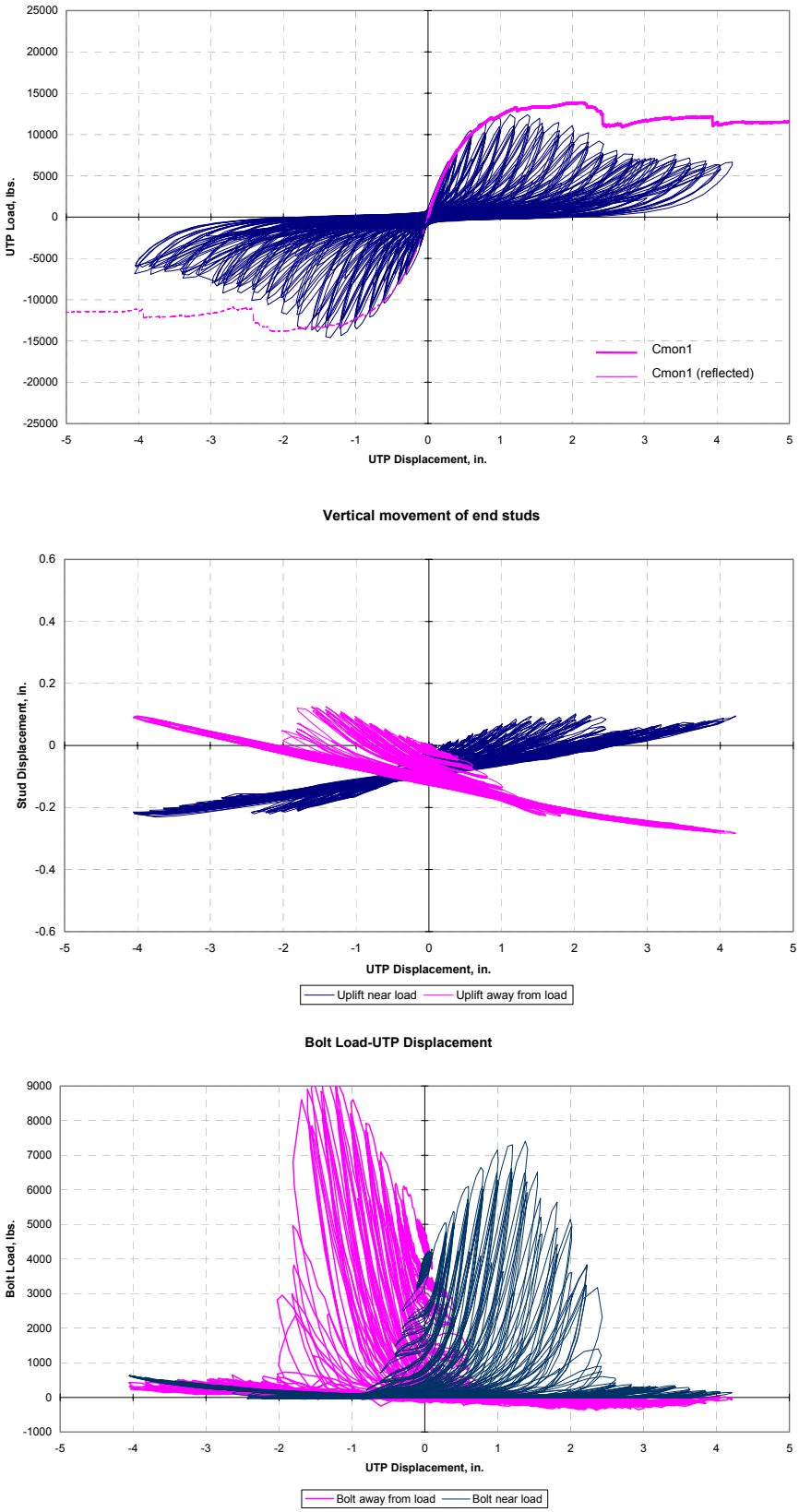

Figure B. 11 - Specimen Ccyc1.

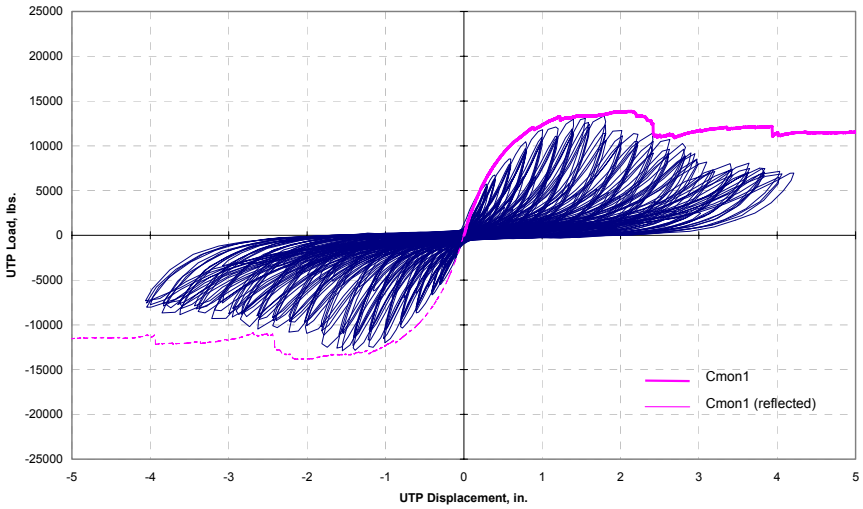

Vertical movement of end studs

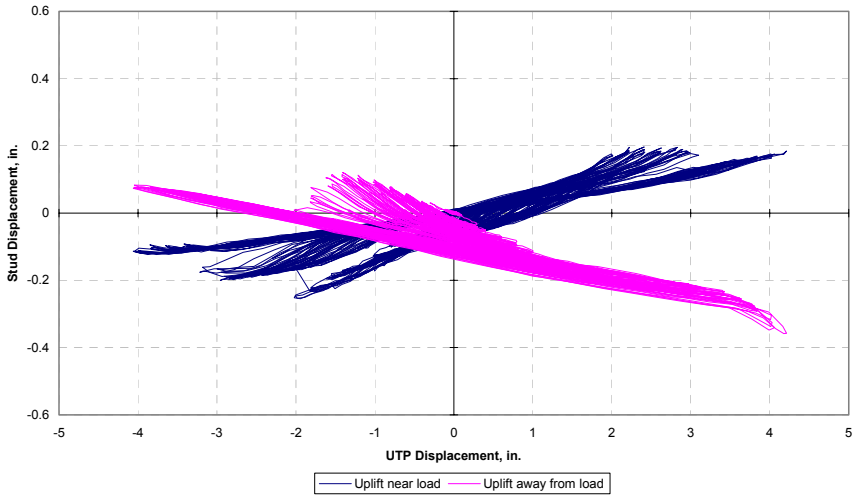

Bolt Load-UTP Displacement

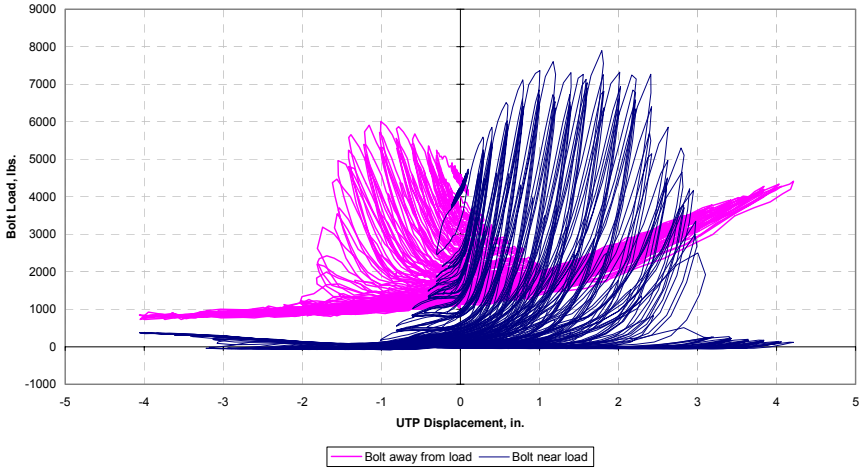

Figure B. 12 - Specimen Ccyc2.

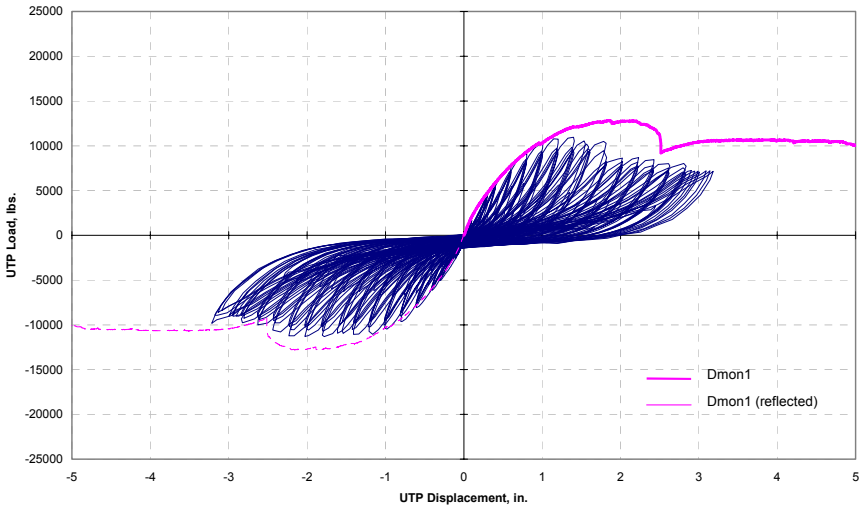

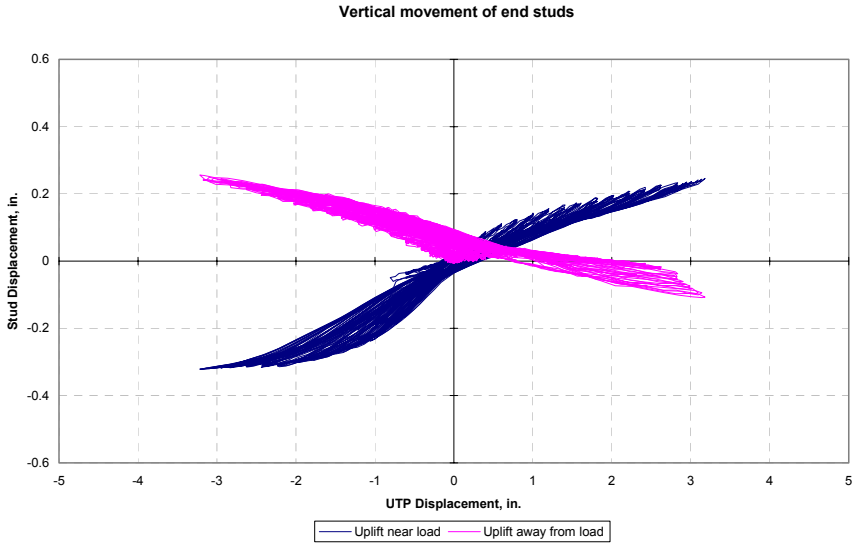

Tension bolts were not installed.

Figure B. 13 - Specimen Dcyc1.

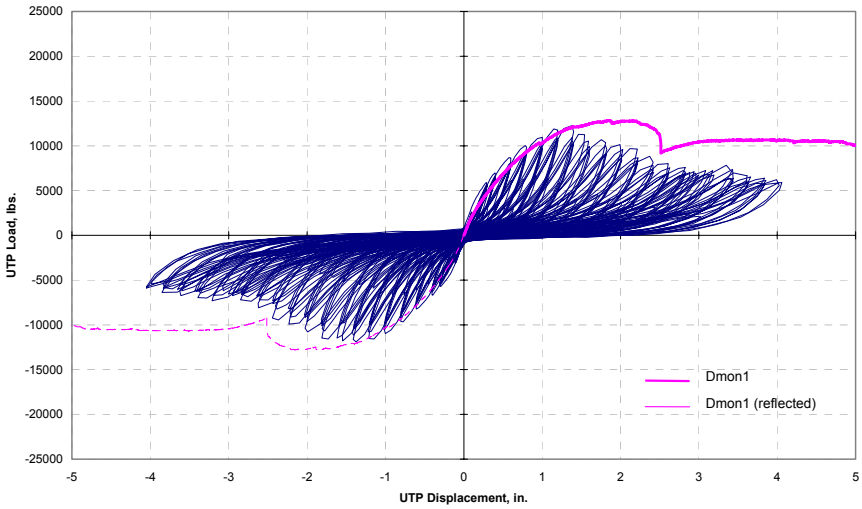

Vertical movement of end studs

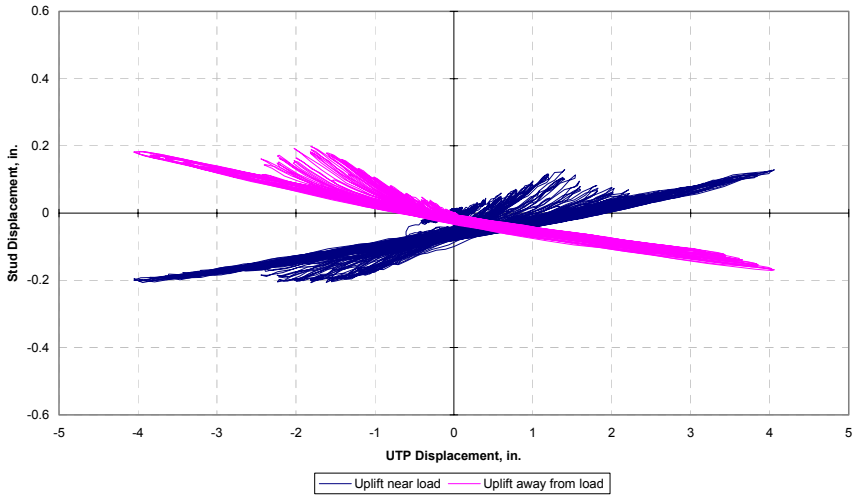

Bolt Load-UTP Displacement

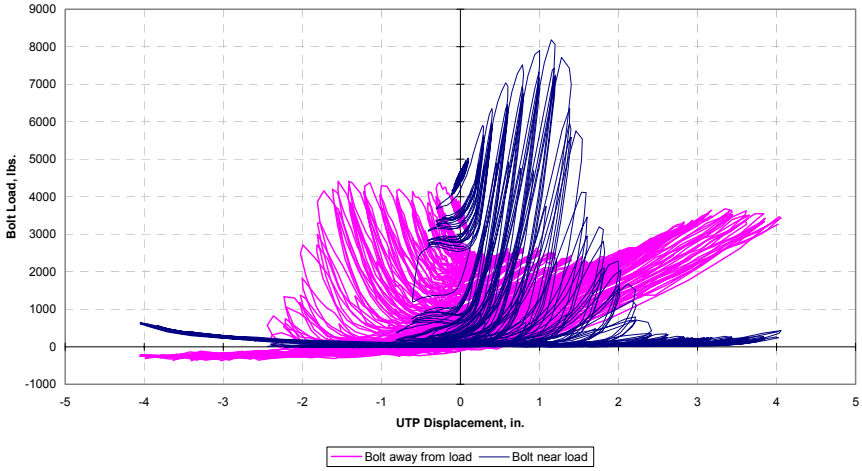

Figure B. 14 - Specimen Dcyc2.

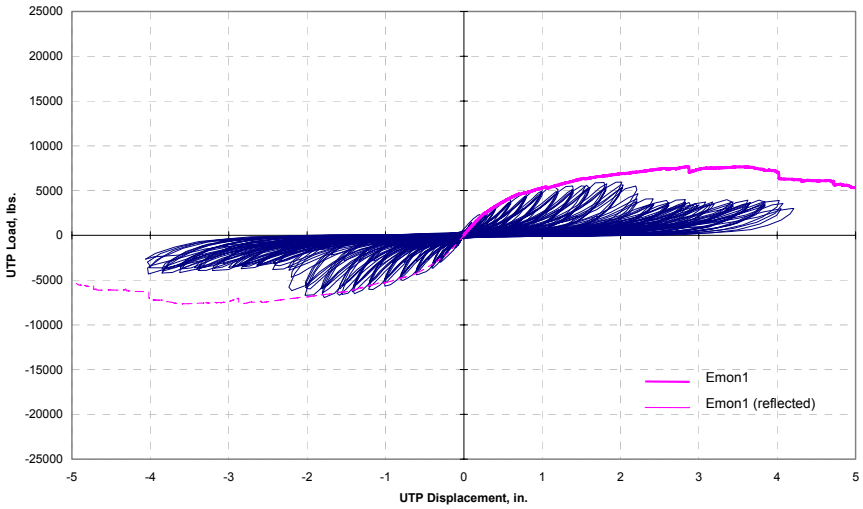

Vertical movement of end studs

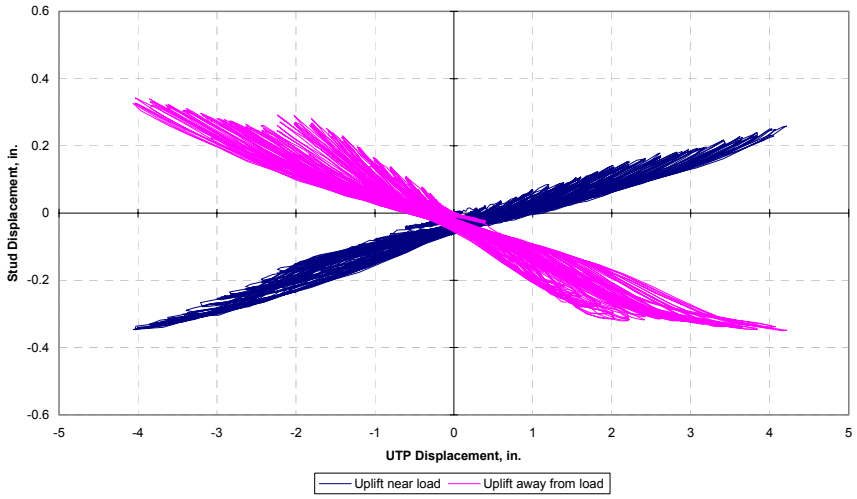

Bolt Load-UTP Displacement

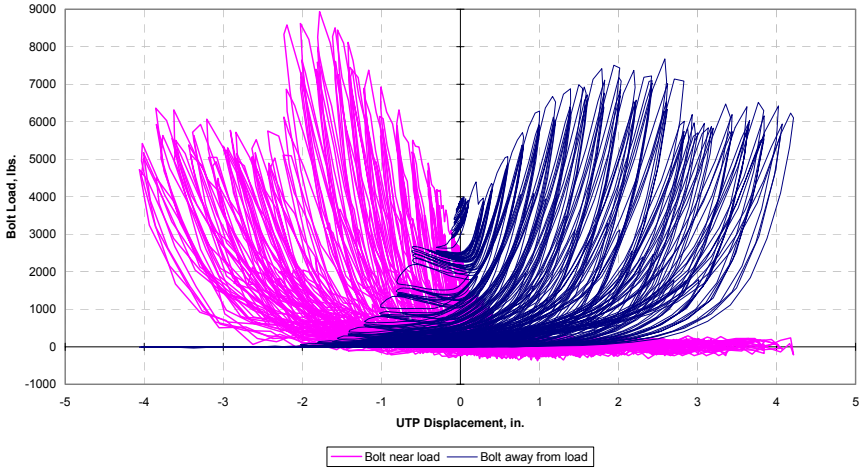

Figure B. 15 - Specimen Ecyc1.

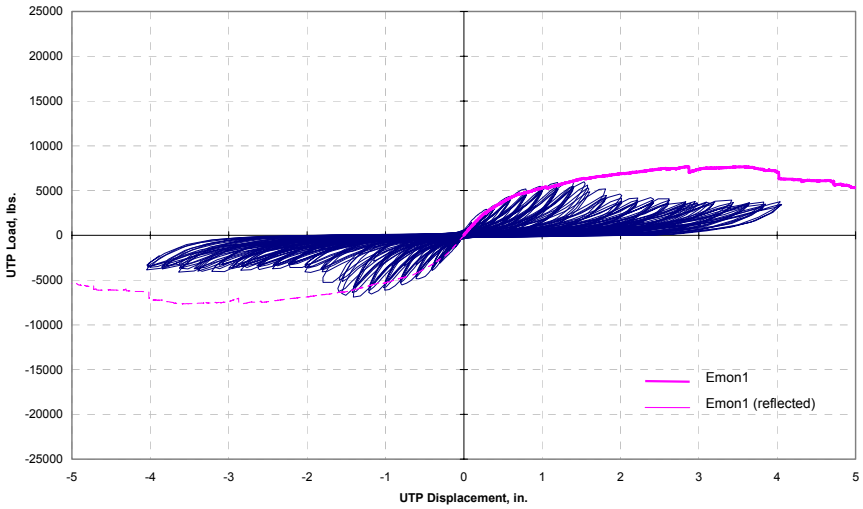

Vertical movement of end studs

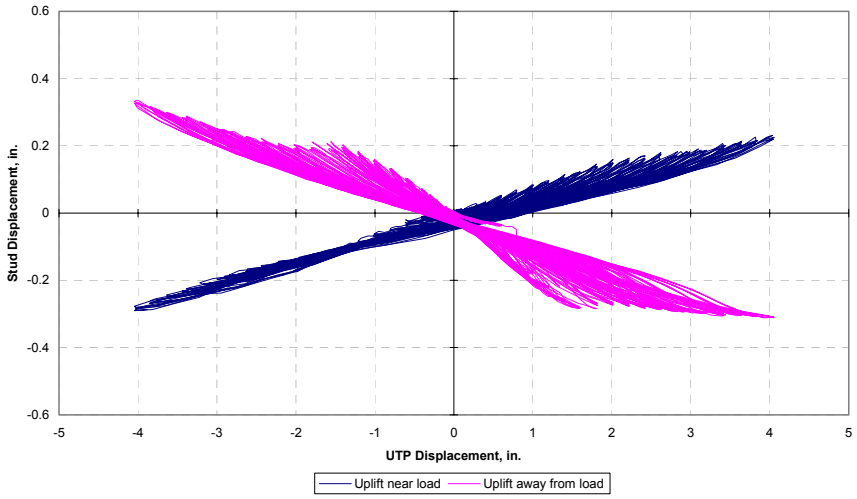

Bolt Load-UTP Displacement

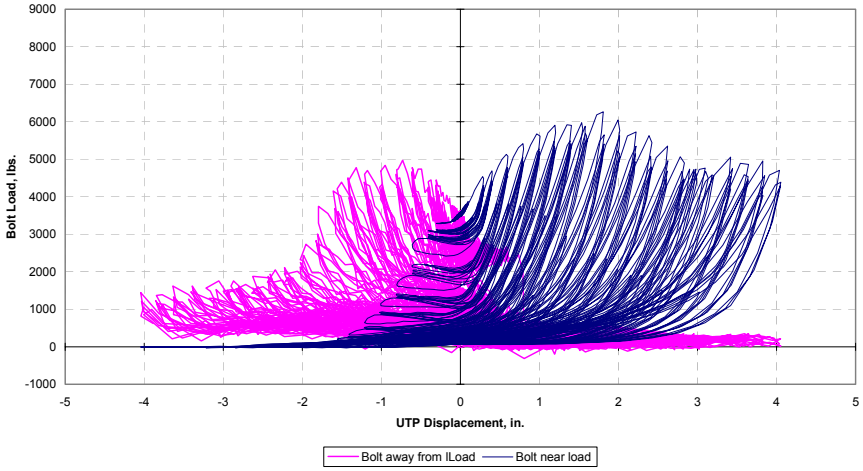

Figure B. 16 - Specimen Ecyc2.

American Iron and Steel Institute

1140 Connecticut Avenue, NW
Suite 705
Washington, DC 20036

www.steel.org

1201 15th Street, NW
Suite 320
Washington, DC 20005

www.steelframing.org

Research Report RP-99-2